In-plane mechanical properties of demi-regular lattice materials

Anastasia Markou, Luc St-Pierre*

Aalto University, Department of Mechanical Engineering, Otakaari 4, 02150 Espoo, Finland.

Abstract

We investigated the potential of demi-regular tessellations to outperform existing prismatic lattice materials, such as the triangular topology. The in-plane mechanical properties of three demi-regular tessellations were derived analytically, and then corroborated by both finite element simulations and experiments. Our analysis showed that these three topologies are elastically isotropic and have a stretching-dominated behaviour. The elastic modulus of these three demi-regular topologies was 5-20% lower than that of a triangular lattice. Demi-regular lattices, however, had a high elastic buckling strength, up to 42% higher than their triangular counterpart. This characteristic makes them ideal topologies for ultra-lightweight applications, where failure is usually governed by elastic buckling.

Keywords: Lattice material, Demi-regular tessellation, Cellular solid, Elastic buckling, Analytical modelling, Finite element analysis

1. Introduction

Prismatic (2D) lattices are particularly attractive for multi-functional applications where both structural efficiency and heat transfer capabilities are required [1, 2]. The most common prismatic lattices are the triangular, hexagonal and square lattices, see Fig. 1. Their elastic modulus and compressive strength have been documented using analytical and numerical methods [3–7] and then, corroborated by experiments [3, 8–11]. This work showed that lattices have either a bending- or a stretching-dominated behaviour depending upon the

*Corresponding Author: luc.st-pierre@aalto.fi

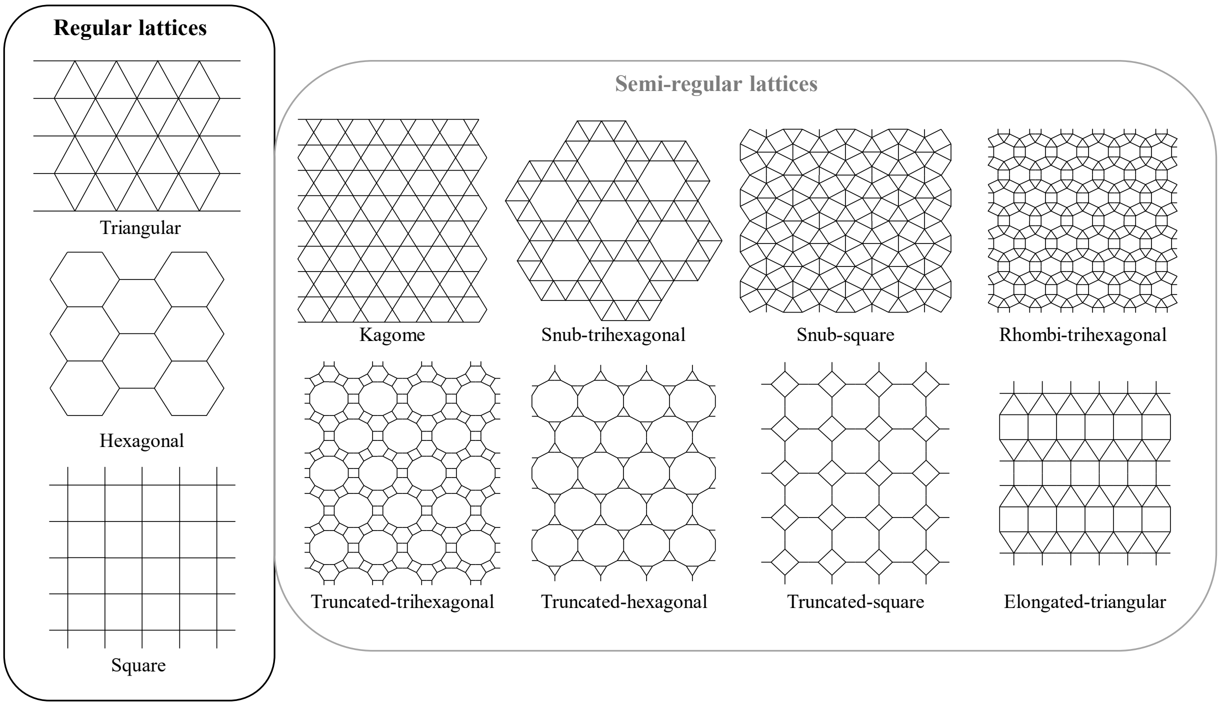

Figure 1: The eleven 1-uniform tessellations include three regular and eight semi-regular lattices. Regular lattices are made from a single regular polygon, whereas semi-regular tessellations are assembled from multiple regular polygons while maintaining a unique vertex configuration.

connectivity of the joints [12]. With three bars per joint, the hexagonal lattice is bending-dominated and consequently, its elastic modulus and yield strength scale as $\bar{\rho}^3$ and $\bar{\rho}^2$, respectively, where $\bar{\rho}$ is the relative density of the lattice [3]. In contrast, the triangular lattice, with six bars per joints, has a stretching-dominated behaviour. Its elastic modulus and yield strength both scale linearly with $\bar{\rho}$, which makes it significantly stiffer and stronger than a hexagonal lattice [5]. At low relative densities, however, the collapse mode of the triangular lattice switches from yielding to elastic buckling, and this is associated with a significant reduction in compressive strength since the buckling resistance scales with $\bar{\rho}^3$ [3, 5, 11]. The development of light, stiff and strong lattice materials would therefore benefit from discovering new topologies that have a stiffness comparable to the triangular lattice, but a higher resistance to elastic buckling. This is the motivation behind this study.

It is insightful to introduce notions of Euclidean tilings to guide the search for new

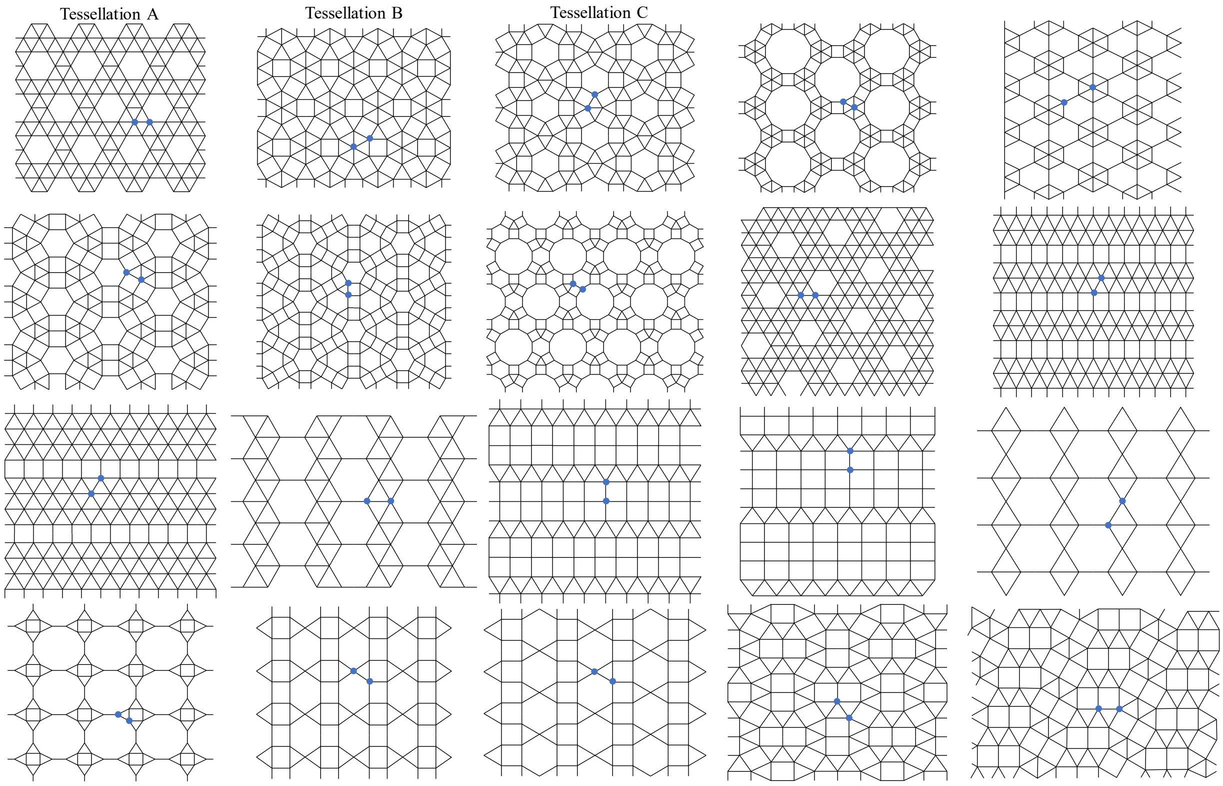

Figure 2: The twenty 2-uniform or demi-regular tessellations. These are assembled from regular polygons and have two different vertex configurations, which are marked in blue.

topologies. Triangular, hexagonal and square topologies are the only three *regular* lattices, defined as tessellations made from a single regular and convex polygon [13]. In contrast, *semi-regular* lattices are assembled from at least two different regular polygons, while maintaining a unique vertex configuration (the sequence of polygons meeting at each joint). There are eight semi-regular lattices [13] and these are shown in Fig. 1. Since both regular and semi-regular lattices have a single vertex configuration, they form a category known as 1-uniform tilings [14]. Tessellations with two different vertex configurations can also be created from regular polygons, and these are called 2-uniform or *demi-regular* lattices. There are 20 demi-regular tessellations [14], and they are given in Fig. 2.

The properties of semi-regular lattices have been reported using analytical and numerical methods [15–21], and two topologies were found to be stretching-dominated: the Kagome and snub-trihexagonal lattices. Even though both tessellations have a higher resistance to elastic buckling than a triangular lattice, their practical use remains limited because (i) the kagome lattice is highly sensitive to imperfections [22, 23], and (ii) the snub-trihexagonal lattice is significantly more compliant than a triangular lattice [21]. These reasons explain why the triangular lattice remains the optimal prismatic topology for high stiffness and strength.

While the properties of semi-regular lattices have been documented, those of demi-regular tessellations remain unknown. Therefore, this study aims to quantify their properties and determine if they can outperform a regular triangular lattice. The scope of this study is limited to three topologies that we will refer to as demi-regular lattices A, B, and C, see Fig. 2. These three tessellations were selected for two reasons. First, they have a six-fold rotational symmetry and therefore, their in-plane elastic properties will be isotropic [24]. Second, they have a high nodal connectivity (4, 5 or 6 bars per joint) and consequently, we expect their behaviour to be stretching-dominated [12]. We will use analytical, numerical, and experimental methods to show that these three demi-regular lattices have a comparable stiffness but a higher resistance to elastic buckling than a triangular lattice.

This article is structured as follows. Analytical equations for the elastic modulus and compressive strength of each demi-regular lattice are derived in Section 2. To validate these analytical expressions, Finite Element (FE) simulations and experiments are developed and described in Section 3. Finally, analytical, numerical, and experimental results are presented in Section 4, where the performances of demi-regular tessellations are compared to those of a regular triangular lattice.

2. Analytical modelling

In this section, analytical expressions are derived for the in-plane elastic modulus, Poisson's ratio and compressive strength of demi-regular lattices A, B, and C, see Fig. 2. Our analysis assumes that all lattices are made from a linear elastic, perfectly plastic material, characterised by a Young's modulus E_s and a yield strength σ_{ys}. All cell walls are considered to have a length ℓ, thickness t, and out-of-plane width b. The cell walls are assumed to behave as trusses since all four lattices are anticipated to be stretching-dominated.

Two collapse mechanisms are considered when deriving the compressive strength of a lattice: yielding and elastic buckling. Yielding occurs when the (tensile or compressive) stress in a cell wall reaches the yield strength σ_{ys}. Otherwise, elastic buckling takes place when the compressive load in a cell wall reaches the Euler buckling load [25]:

$$T_{cr} = \frac{n^2 \pi^2 E_s I}{\ell^2}, \tag{1}$$

where $I = bt^3/12$ is the second moment of area and n is the end constraint factor (for example, $n = 1$ for pinned joints, whereas $n = 2$ when both ends are fixed). The compressive strength of a lattice is governed by the collapse mechanism that has the lowest failure load. Finally, we emphasise that the assumptions detailed above are identical to those used in previous studies [3, 5, 11, 21], which will enable a fair comparison between the properties of these three demi-regular lattices and other tessellations.

2.1. Demi-regular lattice A

Demi-regular lattice A is a tessellation composed of triangles and hexagons, see the unit cell in Fig. 3. Its relative density $\bar{\rho}$ is given by:

$$\bar{\rho} = \frac{14\sqrt{3}}{9}\left(\frac{t}{\ell}\right) = 2.694\left(\frac{t}{\ell}\right). \tag{2}$$

2.1.1. Loading in x_1 direction

Consider demi-regular lattice A loaded in the x_1 direction by a uniform compressive stress σ_1. Because of symmetry, there are only five independent bars and these are labelled on the unit cell shown in Fig. 3. Equilibrium equations for joint A give:

$$T_1 - T_2 + T_3 + 2(T_4 - T_5) = 0, \tag{3}$$

$$T_1 + T_2 - T_3 = 0, \tag{4}$$

where T_i is the internal force in bar i. Otherwise, the macroscopic stress field is $\sigma_{11} = \sigma_1$ and $\sigma_{22} = 0$, and this implies:

$$T_1 + 2(T_2 + T_4 + T_5) = 3\sqrt{3}\sigma_1 b\ell, \tag{5}$$

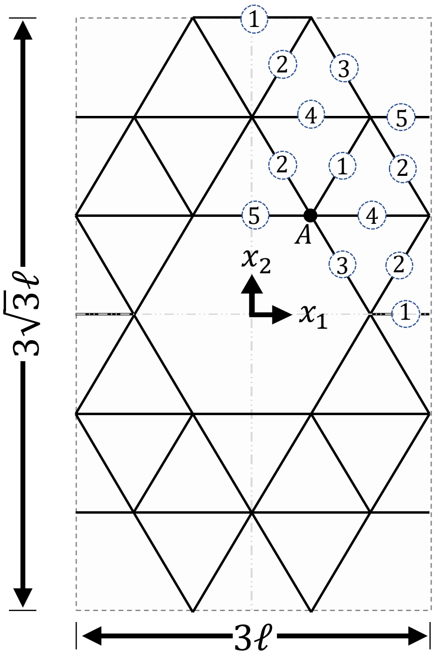

Figure 3: Periodic unit cell of demi-regular lattice A.

$$T_2 + T_3 = 0, \tag{6}$$

respectively. This indeterminate truss can be solved using the principle of minimum strain energy as follows. First, we use (3) to (6) to express T_2, T_3, T_4 and T_5 as functions of T_1. Second, we use these expressions to write the strain energy U as a function of T_1 only. Third, the minimum strain energy is found by setting $\partial U/\partial T_1 = 0$, and this allows to solve for T_1. These steps are detailed in Appendix A.1.1, and return the following internal forces:

$$T_1 = \frac{\sqrt{3}}{10}\sigma_1 b\ell, \tag{7a}$$

$$T_2 = -\frac{\sqrt{3}}{20}\sigma_1 b\ell, \tag{7b}$$

$$T_3 = \frac{\sqrt{3}}{20}\sigma_1 b\ell, \tag{7c}$$

$$T_4 = \frac{7\sqrt{3}}{10}\sigma_1 b\ell, \tag{7d}$$

$$T_5 = \frac{4\sqrt{3}}{5}\sigma_1 b\ell, \tag{7e}$$

where a negative sign (-) indicates tension, whereas a positive value corresponds to compression. Next, the nominal compressive strain in x_1 is given by:

$$\epsilon_1 = \frac{2\Delta_4 + \Delta_5}{3\ell} = \frac{11\sqrt{3}}{15}\frac{\sigma_1}{E_s}\frac{\ell}{t}, \tag{8}$$

where $\Delta_i = T_i\ell/(E_s bt)$ is the extension/shortening of bar i. Therefore, the elastic modulus $E = \sigma_1/\epsilon_1$ becomes:

$$\frac{E}{E_s} = \frac{5\sqrt{3}}{11}\left(\frac{t}{\ell}\right) = 0.292\bar{\rho}. \tag{9}$$

Otherwise, we can find the nominal strain in x_2 using the principle of virtual work, which gives:

$$\epsilon_2 = \frac{1}{15E_s bt}\left(T_1 + 12T_2 + \frac{22}{3}T_3 - 4T_4 - \frac{4}{3}T_5\right) = -\frac{4\sqrt{3}}{15}\frac{\sigma_1}{E_s}\frac{\ell}{t}, \tag{10}$$

and therefore, the Poisson's ratio is:

$$\nu = -\frac{\epsilon_2}{\epsilon_1} = \frac{4}{11} = 0.364. \tag{11}$$

Since this tessellation is isotropic, the shear modulus $G = E/(2(1+\nu))$ and this yields:

$$\frac{G}{E_s} = \frac{\sqrt{3}}{6}\left(\frac{t}{\ell}\right) = 0.107\bar{\rho}. \tag{12}$$

Next, we turn our attention to the compressive strength of demi-regular lattice A. For compression in x_1, bar 5 carries the highest compressive force, see (7). The elastic buckling strength is obtained by equating T_5 to the Euler buckling load in (1), which returns:

$$\frac{\sigma_{1,el}}{E_s} = \frac{5\sqrt{3}}{144}n_1^2\pi^2\left(\frac{t}{\ell}\right)^3 = 0.081\bar{\rho}^3, \tag{13}$$

where the end constraint factor $n_1 = 1.633$ is derived analytically in Appendix B.1. The collapse mode is anticipated to change from elastic buckling to yielding as the relative density increases. The yield strength of the lattice is obtained by setting $T_5 = bt\sigma_{ys}$, which gives:

$$\frac{\sigma_{1,pl}}{\sigma_{ys}} = \frac{5\sqrt{3}}{12}\left(\frac{t}{\ell}\right) = 0.268\bar{\rho}. \tag{14}$$

2.1.2. Loading in x_2 direction

Now, consider demi-regular lattice A loaded in the x_2 direction by uniform compressive stress σ_2. Expressions (3) and (4) remain valid since they represent the equilibrium of joint A, see Fig. 3. Otherwise, enforcing the macroscopic stress field $\sigma_{22} = \sigma_2$ and $\sigma_{11} = 0$ yields:

$$T_2 + T_3 = \sqrt{3}\sigma_2 b\ell, \tag{15}$$

$$T_1 + 2(T_2 + T_4 + T_5) = 0, \tag{16}$$

respectively. The additional equation needed to solve the system is obtained with the principle of minimum strain energy, see Appendix A.1.2, and we find the following internal forces:

$$T_1 = \frac{\sqrt{3}}{10}\sigma_2 b\ell, \tag{17a}$$

$$T_2 = \frac{9\sqrt{3}}{20}\sigma_2 b\ell, \tag{17b}$$

$$T_3 = \frac{11\sqrt{3}}{20}\sigma_2 b\ell, \tag{17c}$$

$$T_4 = -\frac{3\sqrt{3}}{10}\sigma_2 b\ell, \tag{17d}$$

$$T_5 = -\frac{\sqrt{3}}{5}\sigma_2 b\ell. \tag{17e}$$

For compression in x_2, bar 3 carries the highest compressive force. The elastic buckling strength of the lattice is obtained by setting T_3 equal to the Euler buckling load in (1), and this yields:

$$\frac{\sigma_{2,el}}{E_s} = \frac{5\sqrt{3}}{99} n_2^2 \pi^2 \left(\frac{t}{\ell}\right)^3 = 0.094\bar{\rho}^3, \tag{18}$$

where the end constraint factor $n_2 = 1.455$ is derived in Appendix B.1. Otherwise, the yield strength of the lattice is obtained by setting $T_3 = bt\sigma_{ys}$, which gives:

$$\frac{\sigma_{2,pl}}{\sigma_{ys}} = \frac{20\sqrt{3}}{33}\left(\frac{t}{\ell}\right) = 0.390\bar{\rho}. \tag{19}$$

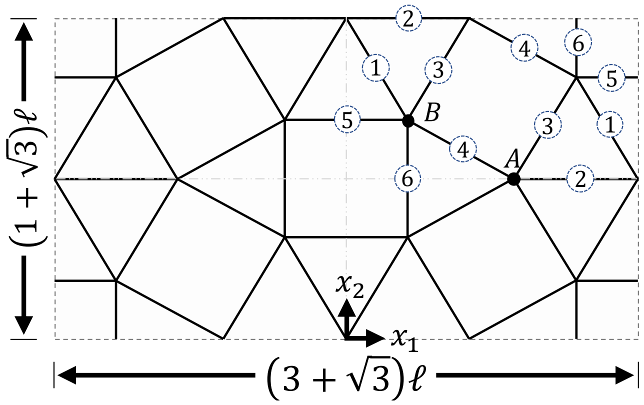

Figure 4: Periodic unit cell of demi-regular lattice B.

2.2. *Demi-regular lattice B*

Demi-regular lattice B is made from triangles and squares as shown on the unit cell in Fig. 4. The relative density of this tessellation is given by:

$$\bar{\rho} = \frac{18}{3 + 2\sqrt{3}} \left(\frac{t}{\ell}\right) = 2.785 \left(\frac{t}{\ell}\right). \tag{20}$$

2.2.1. *Loading in x_1 direction*

First, consider demi-regular lattice B loaded in the x_1 direction by a compressive stress σ_1. This tessellation has six independent bars, which are labelled in Fig. 4. Equilibrium equations for joints A and B give:

$$T_2 + T_3 - \sqrt{3}T_4 = 0, \tag{21}$$

$$T_1 - T_3 - \sqrt{3}T_4 + 2T_5 = 0, \tag{22}$$

$$\sqrt{3}(T_1 + T_3) - T_4 - 2T_6 = 0. \tag{23}$$

Otherwise, the macroscopic stress field is $\sigma_{11} = \sigma_1$ and $\sigma_{22} = 0$ and this implies:

$$T_1 + T_2 + 2T_5 = (1 + \sqrt{3})\sigma_1 b\ell, \tag{24}$$

$$\sqrt{3}(T_1 + T_3) + T_4 + 2T_6 = 0, \tag{25}$$

respectively. Again, demi-regular lattice B is an indeterminate truss and we can use the principle of minimum strain energy to solve the system. Intermediate steps are included in

Appendix A.2.1 and lead to the following internal forces:

$$T_1 = -\frac{(1+\sqrt{3})}{24}\sigma_1 b\ell, \tag{26a}$$

$$T_2 = \frac{11(1+\sqrt{3})}{24}\sigma_1 b\ell, \tag{26b}$$

$$T_3 = \frac{1+\sqrt{3}}{24}\sigma_1 b\ell, \tag{26c}$$

$$T_4 = \frac{3+\sqrt{3}}{6}\sigma_1 b\ell, \tag{26d}$$

$$T_5 = \frac{7(1+\sqrt{3})}{24}\sigma_1 b\ell, \tag{26e}$$

$$T_6 = -\frac{(3+\sqrt{3})}{12}\sigma_1 b\ell. \tag{26f}$$

The nominal compressive strain ϵ_1 is obtained by equating the work done by external loads to the internal strain energy and this gives:

$$\epsilon_1 = \frac{2\sqrt{3}-3}{6E_s\sigma_1 t\ell b^2}\left(8T_1^2 + 4T_2^2 + 8T_3^2 + 8T_4^2 + 4T_5^2 + 4T_6^2\right) = \frac{47\sqrt{3}}{72}\frac{\sigma_1}{E_s}\frac{\ell}{t}. \tag{27}$$

Therefore, the elastic modulus, $E = \sigma_1/\epsilon_1$, of demi-regular lattice B becomes:

$$\frac{E}{E_s} = \frac{24\sqrt{3}}{47}\left(\frac{t}{\ell}\right) = 0.318\bar{\rho}. \tag{28}$$

Otherwise, the nominal strain in x_2 can be calculated using the principle of virtual work, which gives:

$$\epsilon_2 = \frac{3-\sqrt{3}}{18E_s bt}\left(7T_1 - \frac{5}{2}T_2 + 5T_3 - \frac{1}{2}T_5 + 3\sqrt{3}T_6\right) = -\frac{17\sqrt{3}}{72}\frac{\sigma_1}{E_s}\frac{\ell}{t}, \tag{29}$$

and the Poisson's ratio is:

$$\nu = -\frac{\epsilon_2}{\epsilon_1} = \frac{17}{47} = 0.362. \tag{30}$$

Since this tessellation is isotropic, its shear modulus is $G = E/(2(1+\nu))$ and this yields:

$$\frac{G}{E_s} = \frac{3\sqrt{3}}{16}\left(\frac{t}{\ell}\right) = 0.117\bar{\rho}. \tag{31}$$

Next, we turn our attention to the compressive strength of demi-regular lattice B. For compression in x_1, the highest compressive force is in bar 2, see (26). Therefore, the elastic buckling strength is obtained by equating T_2 to the Euler critical load in (1), which returns:

$$\frac{\sigma_{1,el}}{E_s} = \frac{(\sqrt{3}-1)}{11} n_1^2 \pi^2 \left(\frac{t}{\ell}\right)^3 = 0.083\bar{\rho}^3, \tag{32}$$

where the end constraint factor $n_1 = 1.650$ is derived analytically in Appendix B.2. On the other hand, the yield strength of the lattice is obtained by setting $T_2 = bt\sigma_{ys}$, which gives:

$$\frac{\sigma_{1,pl}}{\sigma_{ys}} = \frac{24}{11(1+\sqrt{3})} \left(\frac{t}{\ell}\right) = 0.287\bar{\rho}. \tag{33}$$

2.2.2. Loading in x_2 direction

Now, consider demi-regular lattice B loaded in the x_2 direction by a compressive stress σ_2. Equations (21), (22) and (23) remain valid since they represent the equilibrium of joints A and B, see Fig. 4. On the other hand, enforcing the macroscopic stress field $\sigma_{22} = \sigma_2$ and $\sigma_{11} = 0$ yields:

$$\sqrt{3}(T_1 + T_3) + T_4 + 2T_6 = (3+\sqrt{3})\sigma_2 b\ell, \tag{34}$$

$$T_1 + T_2 + 2T_5 = 0, \tag{35}$$

respectively. The additional equation needed to solve the system is obtained with the principle of minimum strain energy, see Appendix A.2.2, and we find the following internal forces:

$$T_1 = \frac{7(1+\sqrt{3})}{24}\sigma_2 b\ell, \tag{36a}$$

$$T_2 = -\frac{5(1+\sqrt{3})}{24}\sigma_2 b\ell, \tag{36b}$$

$$T_3 = \frac{5(1+\sqrt{3})}{24}\sigma_2 b\ell, \tag{36c}$$

$$T_4 = 0, \tag{36d}$$

$$T_5 = -\frac{(1+\sqrt{3})}{24}\sigma_2 b\ell, \tag{36e}$$

$$T_6 = \frac{(3+\sqrt{3})}{4}\sigma_2 b\ell. \tag{36f}$$

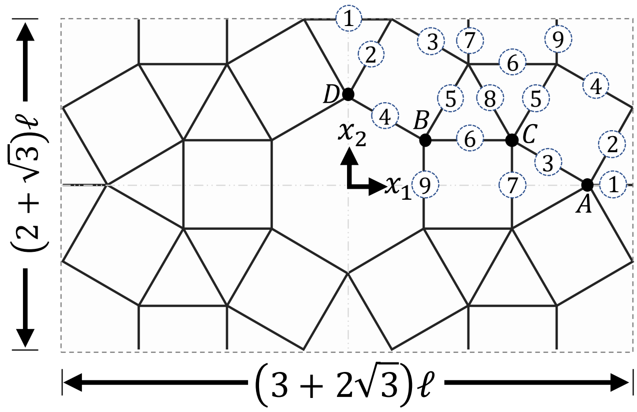

Figure 5: Periodic unit cell of demi-regular lattice C.

Here, bar 6 carries the highest compressive load. Equating T_6 to the Euler critical load in (1) returns the elastic buckling strength of the lattice:

$$\frac{\sigma_{2,el}}{E_s} = \frac{1}{3(3+\sqrt{3})} n_2^2 \pi^2 \left(\frac{t}{\ell}\right)^3 = 0.089\bar{\rho}^3, \tag{37}$$

where the end constraint factor $n_2 = 1.659$ is derived in Appendix B.2. Otherwise, the yield strength is obtained by setting $T_6 = bt\sigma_{ys}$, which gives:

$$\frac{\sigma_{2,pl}}{\sigma_{ys}} = \frac{4}{(3+\sqrt{3})} \left(\frac{t}{\ell}\right) = 0.304\bar{\rho}. \tag{38}$$

2.3. Demi-regular lattice C

Demi-regular lattice C is made from three regular polygons: triangles, squares and hexagons, see its unit cell in Fig. 5. Its relative density is given by:

$$\bar{\rho} = \frac{54}{12+7\sqrt{3}} \left(\frac{t}{\ell}\right) = 2.238 \left(\frac{t}{\ell}\right). \tag{39}$$

2.3.1. Loading in x_1 direction

Consider demi-regular lattice C loaded in the x_1 direction by a uniform compressive stress σ_1. This tessellation has nine independent bars that are labelled in Fig. 5. Equilibrium equations for joints A, B, C and D give:

$$T_1 + T_2 - \sqrt{3}T_3 = 0, \tag{40}$$

$$\sqrt{3}T_4 - T_5 - 2T_6 = 0, \tag{41}$$

$$T_4 + \sqrt{3}T_5 - 2T_9 = 0, \tag{42}$$

$$\sqrt{3}T_3 + T_5 - 2T_6 - T_8 = 0, \tag{43}$$

$$-T_3 + \sqrt{3}(T_5 + T_8) - 2T_7 = 0, \tag{44}$$

$$\sqrt{3}T_2 - T_4 = 0. \tag{45}$$

Otherwise, the macroscopic stress field is $\sigma_{11} = \sigma_1$ and $\sigma_{22} = 0$, which implies that:

$$T_1 + T_2 + \sqrt{3}T_4 = (2 + \sqrt{3})\sigma_1 b\ell, \tag{46}$$

$$\sqrt{3}T_2 + T_3 + 2(T_7 + T_9) = 0. \tag{47}$$

Again, the additional equation needed to solve the system is obtained using the principle of minimum strain energy. Intermediate steps are included in Appendix A.3.1 and lead to the following internal forces:

$$T_1 = \frac{11(2+\sqrt{3})}{24}\sigma_1 b\ell, \tag{48a}$$

$$T_2 = \frac{13(2+\sqrt{3})}{96}\sigma_1 b\ell, \tag{48b}$$

$$T_3 = \frac{19(3+2\sqrt{3})}{96}\sigma_1 b\ell, \tag{48c}$$

$$T_4 = \frac{13(3+2\sqrt{3})}{96}\sigma_1 b\ell, \tag{48d}$$

$$T_5 = -\frac{11(2+\sqrt{3})}{96}\sigma_1 b\ell, \tag{48e}$$

$$T_6 = \frac{25(2+\sqrt{3})}{96}\sigma_1 b\ell, \tag{48f}$$

$$T_7 = -\frac{17(3+2\sqrt{3})}{96}\sigma_1 b\ell, \tag{48g}$$

$$T_8 = -\frac{(2+\sqrt{3})}{24}\sigma_1 b\ell, \tag{48h}$$

$$T_9 = \frac{(3+2\sqrt{3})}{96}\sigma_1 b\ell. \tag{48i}$$

The nominal compressive strain ϵ_1 is obtained by equating the work done by external loads to the internal strain energy, which gives:

$$\epsilon_1 = \frac{7\sqrt{3}-12}{3E_s\sigma_1 t\ell b^2}\left(2T_1^2 + 8\left(T_2^2 + T_3^2 + T_4^2 + T_5^2 + T_6^2\right) + 4\left(T_7^2 + T_8^2 + T_9^2\right)\right)$$

$$= \frac{143\sqrt{3}}{144}\frac{\sigma_1}{E_s}\frac{\ell}{t}. \tag{49}$$

Therefore, the elastic modulus $E = \sigma_1/\epsilon_1$ becomes:

$$\frac{E}{E_s} = \frac{48\sqrt{3}}{143}\left(\frac{t}{\ell}\right) = 0.260\bar{\rho}. \tag{50}$$

Otherwise, the nominal strain along x_2 can be calculated using the principle of virtual work, which gives:

$$\epsilon_2 = \frac{2-\sqrt{3}}{6E_s bt}\left(-\frac{5\sqrt{3}}{6}(T_1 - T_2) - \frac{5}{2}(T_3 - T_4) + \frac{\sqrt{3}}{6}(29T_5 - 7T_6)\right. \\ \left. + \frac{31}{4}T_7 + \frac{7\sqrt{3}}{3}T_8 + \frac{17}{4}T_9\right) = -\frac{65\sqrt{3}}{144}\frac{\sigma_1}{E_s}\frac{\ell}{t}, \tag{51}$$

and the Poisson's ratio is:

$$\nu = -\frac{\epsilon_2}{\epsilon_1} = \frac{65}{143} = 0.455. \tag{52}$$

Since this tessellation is isotropic, the shear modulus is $G = E/(2(1+\nu))$ and this yields:

$$\frac{G}{E_s} = \frac{3\sqrt{3}}{26}\left(\frac{t}{\ell}\right) = 0.089\bar{\rho}. \tag{53}$$

Next, we turn our attention to the compressive strength of demi-regular lattice C. For compression in x_1, the maximum compressive load is in bar 1, see (48). Equating T_1 to the Euler buckling load in (1) gives us the elastic buckling strength of the lattice:

$$\frac{\sigma_{1,el}}{E_s} = \frac{2(2-\sqrt{3})}{11}n_1^2\pi^2\left(\frac{t}{\ell}\right)^3 = 0.105\bar{\rho}^3, \tag{54}$$

where the end constraint factor $n_1 = 1.567$ is derived analytically in Appendix B.3. In contrast, the yield strength is obtained by setting $T_1 = bt\sigma_{ys}$, which gives:

$$\frac{\sigma_{1,pl}}{\sigma_{ys}} = \frac{24(2-\sqrt{3})}{11}\left(\frac{t}{\ell}\right) = 0.261\bar{\rho}. \tag{55}$$

2.3.2. Loading in x_2 direction

Now, consider demi-regular lattice C loaded in the x_2 direction by a uniform compressive stress σ_2. Expressions (40) to (45) remain valid since they represent the equilibrium of joints A, B, C and D, see Fig. 5. Otherwise, enforcing the macroscopic stress field $\sigma_{22} = \sigma_2$ and $\sigma_{11} = 0$, yields:

$$\sqrt{3}T_2 + T_3 + 2(T_7 + T_9) = (3 + 2\sqrt{3})\sigma_2 b\ell, \tag{56}$$

$$T_1 + T_2 + \sqrt{3}T_4 = 0, \tag{57}$$

respectively. The additional equation needed to solve the system is obtained with the principle of minimum strain energy, see Appendix A.3.2, and we find the following internal forces:

$$T_1 = -\frac{5(2+\sqrt{3})}{24}\sigma_2 b\ell, \tag{58a}$$

$$T_2 = \frac{5(2+\sqrt{3})}{96}\sigma_2 b\ell, \tag{58b}$$

$$T_3 = -\frac{5(3+2\sqrt{3})}{96}\sigma_2 b\ell, \tag{58c}$$

$$T_4 = \frac{5(3+2\sqrt{3})}{96}\sigma_2 b\ell, \tag{58d}$$

$$T_5 = \frac{29(2+\sqrt{3})}{96}\sigma_2 b\ell, \tag{58e}$$

$$T_6 = -\frac{7(2+\sqrt{3})}{96}\sigma_2 b\ell, \tag{58f}$$

$$T_7 = \frac{31(3+2\sqrt{3})}{96}\sigma_2 b\ell, \tag{58g}$$

$$T_8 = \frac{7(2+\sqrt{3})}{24}\sigma_2 b\ell, \tag{58h}$$

$$T_9 = \frac{17(3+2\sqrt{3})}{96}\sigma_2 b\ell. \tag{58i}$$

Here, the highest compressive force is in bar 7. Therefore, the elastic buckling strength is obtained by equating T_7 to the Euler buckling load in (1), which gives:

$$\frac{\sigma_{2,el}}{E_s} = \frac{8(2\sqrt{3}-3)}{93}n_2^2\pi^2\left(\frac{t}{\ell}\right)^3 = 0.098\bar{\rho}^3, \tag{59}$$

where the end constraint factor $n_2 = 1.667$ is derived analytically in Appendix B.3. Otherwise, the yield strength of the lattice is obtained by setting $T_7 = bt\sigma_{ys}$, which yields:

$$\frac{\sigma_{2,pl}}{\sigma_{ys}} = \frac{32(2\sqrt{3}-3)}{31}\left(\frac{t}{\ell}\right) = 0.214\bar{\rho}. \tag{60}$$

3. Materials and methods

Both Finite Element (FE) simulations and experiments were conducted to verify the analytical expressions derived in Section 2. Below, our FE modelling approach is presented first, followed by a description of our experimental protocol.

3.1. Finite element modelling

All simulations were done with the commercial software Abaqus and using the standard solver (Static, Implicit step). Periodic unit cells, identical to those in Fig. 3 to 5, were used for each topology. In all cases, the bar length was kept fixed to $\ell = 10$ mm, but the bar thickness t was varied to cover a range of relative densities $\bar{\rho}$ from 0.01 to 0.3. Each bar was discretised using at least 70 Timoshenko beam elements (B21 in Abaqus notation) based on a mesh convergence study (not shown here). It was necessary to include a geometric imperfection in all simulations to trigger buckling. This imperfection had the shape of the first non-swaying eigenmode and its amplitude was set to 5% of the bar thickness, as used in previous studies on prismatic lattices [11, 21].

The parent material was modelled as an elastic perfectly plastic solid. The elastic regime was linear and isotropic, characterised by a Young's modulus $E_s = 200$ GPa and a Poisson's ratio $\nu_s = 0.26$, up to a yield strength $\sigma_{ys} = 250$ MPa. These material properties, representative of steel, were selected to ensure that both collapse modes (elastic buckling and yielding) occur over the range of relative densities considered ($0.01 \leq \bar{\rho} \leq 0.3$).

Periodic boundary conditions were imposed on each unit cell using the following constraint equations [7, 11, 21]:

$$\Delta u_i = \epsilon_{ij}\Delta x_j \quad \text{and} \quad \Delta\phi = 0, \tag{61}$$

where Δu_i and $\Delta\phi$ are the difference in displacement and rotation, respectively, between corresponding points of the unit cell; ϵ_{ij} is the macroscopic nominal strain tensor; and Δx_j is the displacement vector connecting two corresponding points of the unit cell. The compressive response of the lattice along x_1 was obtained by prescribing ϵ_{11}, and letting Abaqus calculate σ_{11} assuming $\sigma_{22} = 0$. Likewise, the compressive response in x_2 was obtained by imposing ϵ_{22}, and computing σ_{22} provided $\sigma_{11} = 0$. Finally, the response in shear was obtained by prescribing ϵ_{12} and computing σ_{12} while keeping $\sigma_{11} = \sigma_{22} = 0$.

3.2. Specimen manufacture and compression tests

Experiments were designed to (i) corroborate the analytical expressions derived in Section 2 and (ii) compare the performances of demi-regular tessellations to those of a regular triangular lattice. All samples were produced by additive manufacturing using a Formlabs Form 3 machine, which relies on stereolithography to cure a photo-polymerising resin. The overall dimensions of each lattice are given in Fig. 6. All samples had a relative density $\bar{\rho} = 0.17$, and this was achieved by keeping the bar length fixed at $\ell = 10$ mm and adjusting the strut thickness t as indicated in Table 1. In all cases, the specimens had a depth of 25 mm in the prismatic direction. The samples were compressed only in the x_2 direction since they are elastically isotropic and this is the strongest orientation for all topologies (except tessellation C where the elastic buckling strength is 7% higher in x_1, see Section 2).

The specimens were fabricated as follows. First, the geometry of the sample was created in Abaqus and a stl file was exported to the Form 3 printer. Second, the specimen was printed with a layer thickness of 0.05 mm and using Formlabs Clear resin. All samples were printed with their prismatic axis perpendicular to the printing bed. Finally, when the print was completed, the lattice was washed in an isopropyl alcohol (IPA) solution and post-cured under UV light at a temperature of 60°C for 30 min, as recommended in the Formlabs documentation. The printed lattices had no visible imperfections, such as broken or wavy bars. All samples were compressed at rate of 0.05 mm/s using a MTS electromechanical testing machine with a capacity of 30 kN. Both the compressive force and displacement were recorded by the testing machine.

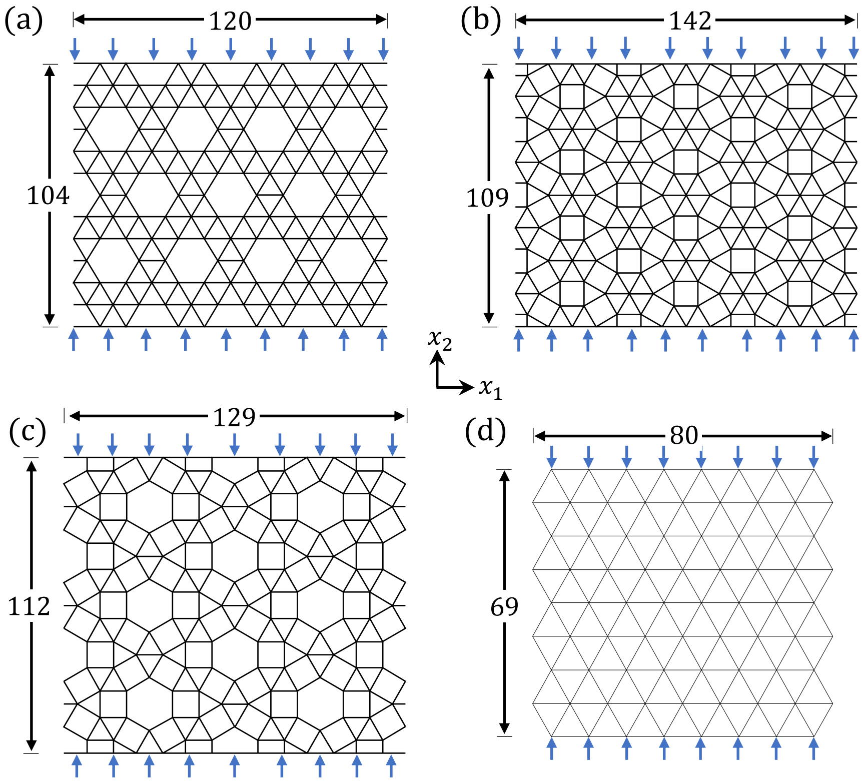

Figure 6: Dimensions, in mm, of the tested samples: demi-regular tessellations (a) A, (b) B, and (c) C as well as (d) a triangular lattice. All samples had a bar length $\ell = 10$ mm and a depth of 25 mm in the prismatic direction.

Table 1: Values of relative density $\bar{\rho}$, bar thickness t, and bar length ℓ used in the experiments.

Topology	$\bar{\rho}$	t [mm]	ℓ [mm]	t/ℓ
A	0.17	0.63	10	0.063
B	0.17	0.61	10	0.061
C	0.17	0.76	10	0.076
Triangular	0.17	0.49	10	0.049

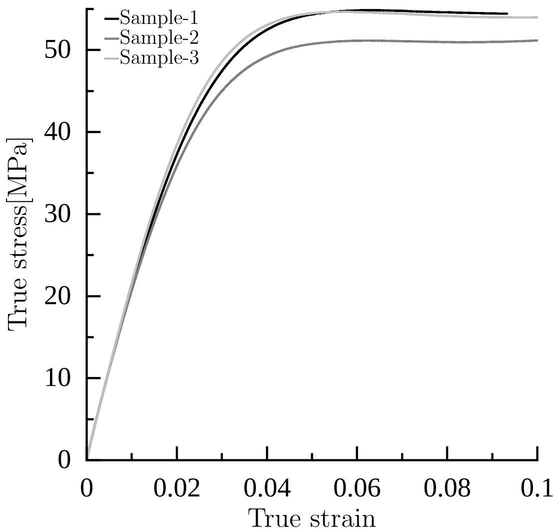

Figure 7: Responses of three tensile tests done on the polymer used to manufacture all lattices.

Tensile tests were conducted to characterise the behaviour of the Clear resin used to manufacture all lattices. Following the procedure detailed above, three tensile specimens were printed with a thickness of 0.6 mm and a gauge length of 15 mm (dimensions comparable to those of a cell wall inside the lattice samples). The tensile responses, measured at a strain rate of $5 \cdot 10^{-4}\,\mathrm{s}^{-1}$, are shown in Fig. 7. The measurements have a small scatter with an average Young's modulus $E_s = 2.1\,\mathrm{GPa}$ and a mean ultimate tensile strength of 54 MPa.

4. Results and discussion

Our results are presented below in three parts. First, numerical and analytical results are compared to validate the expressions derived in Section 2. Second, we use our analytical results to compare the properties of demi-regular tessellations to those of a triangular lattice. Third, we present our experimental results to corroborate the performances of demi-regular tessellations.

4.1. Comparison between analytical and finite element results

Finite Element (FE) simulations are compared to analytical predictions in Fig. 8a for the elastic modulus E and in Fig. 8b for the shear modulus G. Both moduli are normalised by the Young's modulus of the solid E_s; hence, the results in Fig. 8 are insensitive to the choice

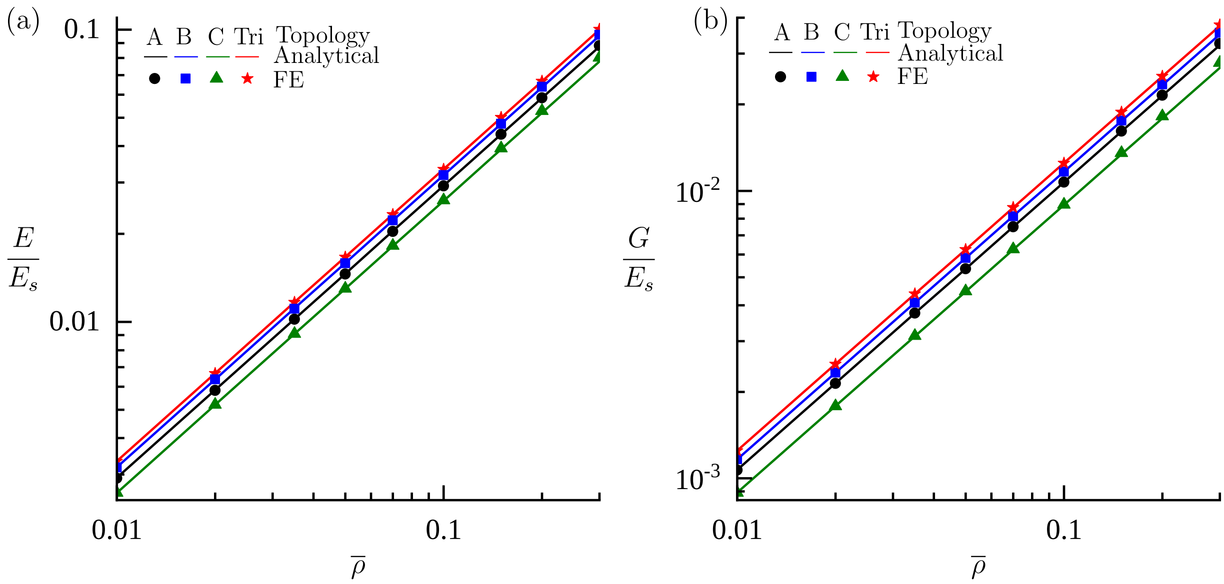

Figure 8: Comparison between analytical and FE results: (a) elastic modulus E and (b) shear modulus G, both plotted as a function of relative density $\bar{\rho}$ and normalised by the Young's modulus of the parent material $E_s = 200\,\text{GPa}$. Results for demi-regular tessellations A, B, and C are compared to those of a triangular lattice.

of parent material. Results are given for all three demi-regular lattices. In all cases, there is an excellent agreement between FE and analytical results for both E and G. This is true over the entire range of relative density considered here ($0.01 \leq \bar{\rho} \leq 0.3$).

Next, FE predictions of the compressive strength are compared to analytical results in Fig. 9a and b for compression in x_1 and x_2, respectively. Here, the compressive strength is normalised by the yield strength $\sigma_{ys} = 250\,\text{MPa}$ of the parent material. In all cases, the collapse mode changes from elastic buckling (at low relative densities) to yielding (at high values of $\bar{\rho}$) and this transition is noticeable in Fig. 9 by the change in slope. For both collapse modes, there is an excellent agreement between FE and analytical results. This holds true for both loading directions, and for all three demi-regular lattices.

Even though analytical and FE models share similar assumptions (both rely on periodic unit cells and consider an elastic, perfectly plastic parent material), there is an important difference. The simulations are done using Timoshenko beam elements, which account for axial, bending and shear deformations. In contrast, our analytical model assumes that

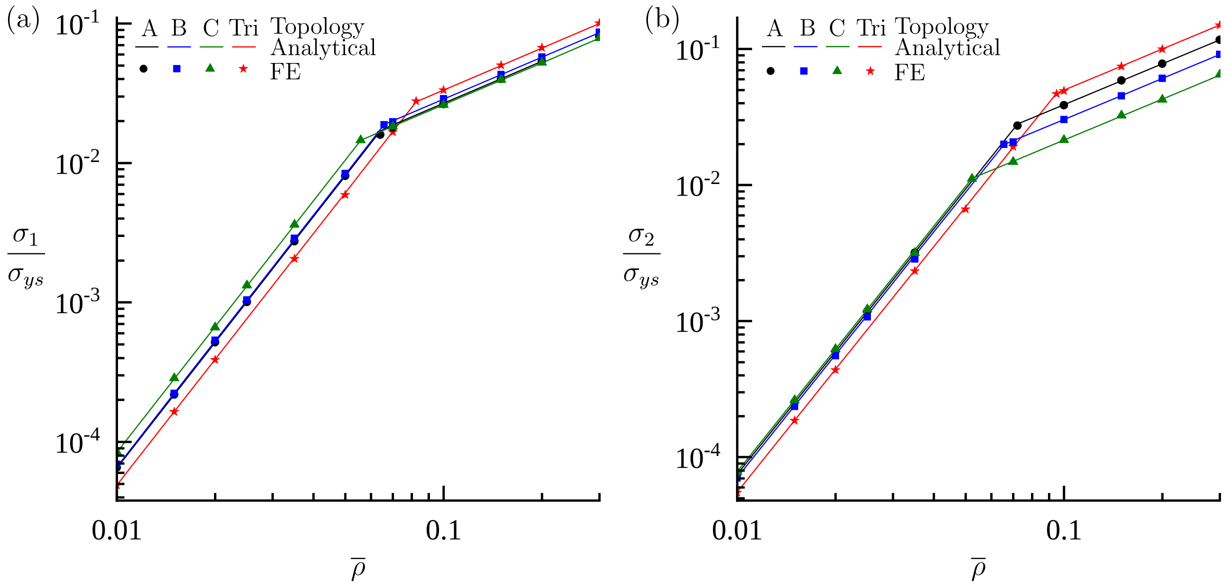

Figure 9: Comparison between analytical and FE results for the normalised compressive strength in (a) x_1 and (b) x_2 directions, both plotted as a function of relative density $\bar{\rho}$. Results for demi-regular tessellations A, B, and C are compared to those of a triangular lattice. The properties of the parent material are $E_s = 200\,\mathrm{GPa}$ and $\sigma_{ys} = 250\,\mathrm{MPa}$.

each bar behaves as a pin-jointed truss, neglecting bending and shear deformations. This assumption is justified based on the excellent agreement between FE and analytical results in Fig. 8 and 9. Therefore, we conclude that the analytical expressions derived in Section 2 are validated by FE simulations.

4.2. Comparison between demi-regular and triangular lattices

4.2.1. Analytical results

Now that our analytical equations are verified, we can use them to compare the performances of demi-regular tessellations to those of a triangular lattice. This is a fair comparison since these four topologies are stretching-dominated and in-plane elastically isotropic. The mechanical properties of demi-regular tessellations A, B, and C are compared to those of a triangular lattice in Fig. 8 and 9, as well as in Table 2, where all analytical expressions are summarised. Here, the properties of a triangular lattice are collected from previous studies [3–6, 11] and its orientation is defined in Fig. 6d.

Demi-regular lattices have a comparable, yet slightly lower elastic modulus E than a

Table 2: The mechanical properties of demi-regular tessellations A, B, and C are compared to those of a triangular lattice. The properties of a triangular lattice are collected from [3–6, 11].

Topology	$\bar{\rho}$	E/E_s	ν	G/E_s	$\sigma_{1,el}/E_s$	$\sigma_{2,el}/E_s$	$\sigma_{1,pl}/\sigma_{ys}$	$\sigma_{2,pl}/\sigma_{ys}$
A	$2.694\,t/\ell$	$0.292\bar{\rho}$	0.364	$0.107\bar{\rho}$	$0.081\bar{\rho}^3$	$0.094\bar{\rho}^3$	$0.268\bar{\rho}$	$0.390\bar{\rho}$
B	$2.785\,t/\ell$	$0.318\bar{\rho}$	0.362	$0.117\bar{\rho}$	$0.083\bar{\rho}^3$	$0.089\bar{\rho}^3$	$0.287\bar{\rho}$	$0.304\bar{\rho}$
C	$2.238\,t/\ell$	$0.260\bar{\rho}$	0.455	$0.089\bar{\rho}$	$0.105\bar{\rho}^3$	$0.098\bar{\rho}^3$	$0.261\bar{\rho}$	$0.214\bar{\rho}$
Triangular	$3.464\,t/\ell$	$0.333\bar{\rho}$	0.333	$0.125\bar{\rho}$	$0.061\bar{\rho}^3$	$0.069\bar{\rho}^3$	$0.333\bar{\rho}$	$0.500\bar{\rho}$

triangular lattice, see Table 2 and Fig. 8a. Tessellation B has the highest elastic modulus, being only 5% more compliant than a triangular lattice, followed by topologies A and then C. These observations also hold true for the shear modulus G.

The triangular lattice has a higher yield strength than any of the three demi-regular lattices, see Table 2 and Fig. 9. For compression in x_1, all three demi-regular topologies have a similar yield strength, which is 15-20% lower than a triangular lattice, see Fig. 9a. When compressed in x_2, demi-regular lattice A has the highest yield strength, yet it remains 20% lower than a triangular lattice.

The main advantage of demi-regular lattices is their high resistance to elastic buckling, see Table 2 and Fig. 9. All demi-regular lattices have a significantly higher elastic buckling strength than a triangular lattice, and this holds true for both compression in x_1 and x_2. The elastic buckling strength in x_2 is greater than that in x_1, except for tessellation C. Nonetheless, demi-regular lattice C offers the highest elastic buckling strength in x_2, being 42% stronger than a triangular lattice. Amongst demi-regular lattices, tessellation B has the lowest elastic buckling strength $\sigma_{2,el}$, yet it remains about 30% stronger than a triangular lattice.

In summary, our analytical results show that demi-regular tessellations are slightly more compliant but significantly stronger than a triangular lattice when failure is governed by elastic buckling. In the next section, experiments are presented to corroborate these findings.

4.2.2. Experimental results

The measured compressive responses are plotted in Fig. 10 for demi-regular tessellations A, B, and C as well as for a triangular lattice. All tests have a linear elastic regime up to a peak stress, followed by a gradual softening response. All lattices failed by elastic buckling

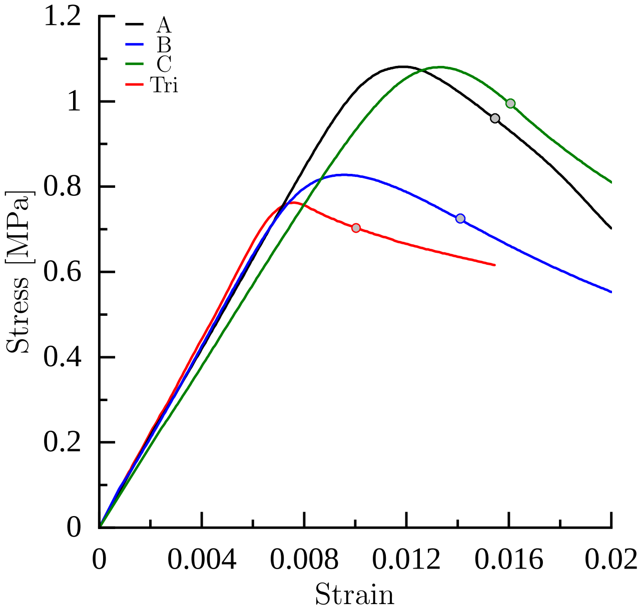

Figure 10: The measured compressive responses of demi-regular tessellations A, B, and C are compared to that of a triangular lattice. All samples have a relative density $\bar{\rho} = 0.17$.

and their deformation is shown in Fig. 11. Buckling took place in the diagonal bars for tessellation A and the triangular lattice (see Fig. 11a,d), whereas the vertical struts buckled in demi-regular lattices B and C (see Fig. 11b,c). These deformation modes are in good agreement with the periodic buckling patterns considered in our analytical model, which are included in Fig. 11 for comparison.

Two tests were done for each topology and the elastic modulus and compressive strength measured are summarised in Fig. 12a and b, respectively. Here, the elastic modulus E is normalised by $E_s = 2.1\,\mathrm{GPa}$, whereas the compressive strength is normalised by $\sigma_{ys} = 54\,\mathrm{MPa}$ (see the tensile response of the parent material in Fig. 7). The experiments have a good repeatability, with variations inferior to 10%, except for tessellation A which shows a larger disparity between tests. Taking the average of both tests, the experimental results indicate that demi-regular lattice B is 5% more compliant than a triangular lattice, whereas this value increases to 13% for tessellation C. The tests also show that demi-regular lattice C is 47% stronger than a triangular lattice. These differences in elastic modulus and compressive strength are in-line with with our analytical predictions, see Table 2.

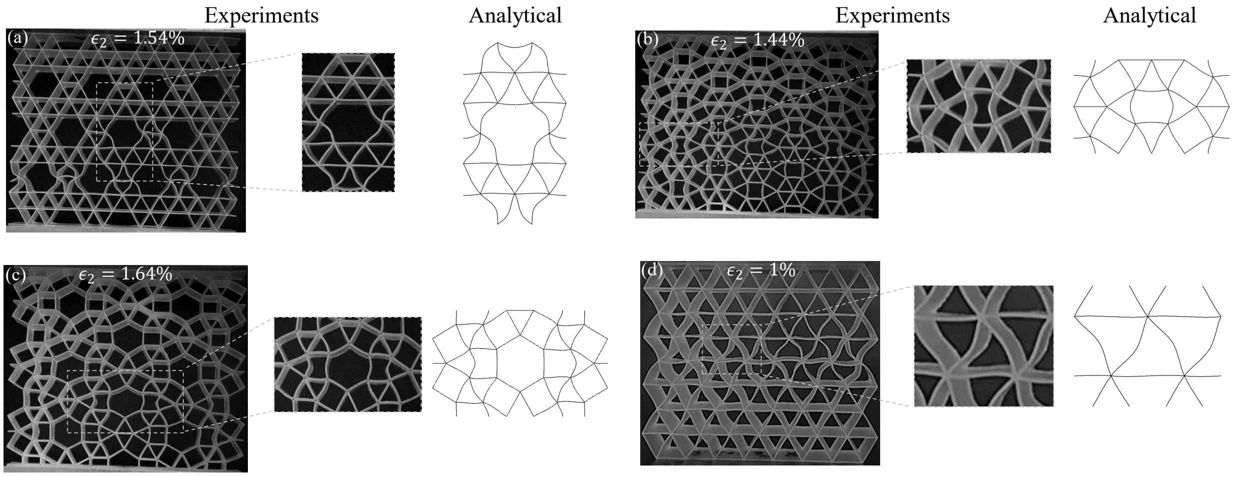

Figure 11: Photographs showing the deformation modes of demi-regular tessellations (a) A, (b) B, and (c) C, as well as (d) a triangular lattice. All lattices have a relative density $\bar{\rho} = 0.17$ and fail by elastic buckling. The instant when each photograph was taken is indicated on the responses in Fig. 10 with a circular symbol. For scale, all bars have a length of 10 mm. For each topology, the period buckling shape considered in our analytical model is also included for comparison.

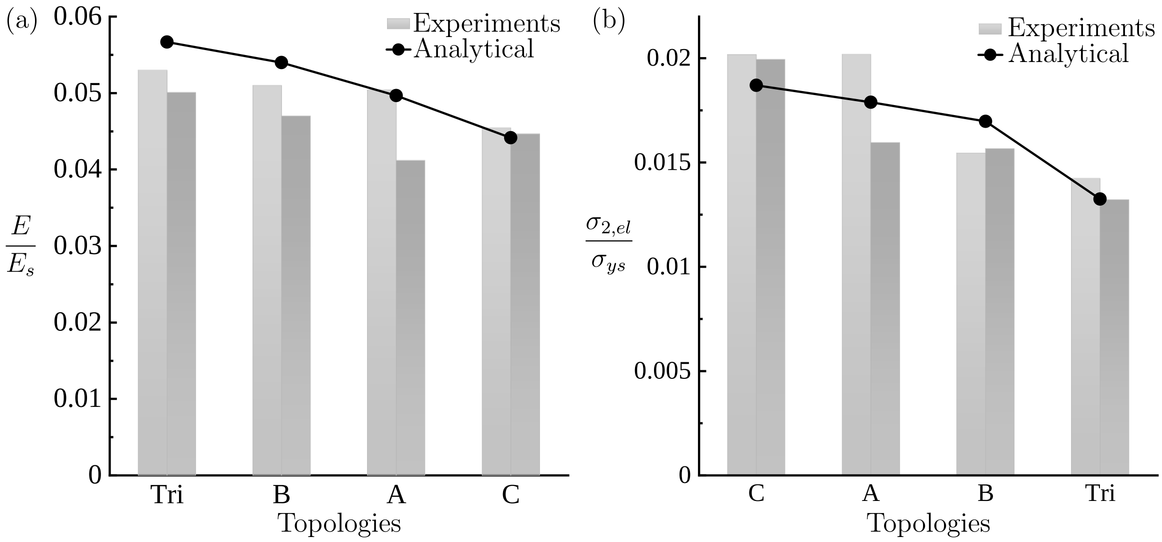

Figure 12: Comparison between experimental and analytical results: (a) normalised elastic modulus and (b) normalised compressive strength in x_2. Results are given for demi-regular tessellations A, B, and C, as well as a triangular lattice. In all cases, the relative density is $\bar{\rho} = 0.17$ and the properties of the parent material are $E_s = 2.1\,\mathrm{GPa}$ and $\sigma_{ys} = 54\,\mathrm{MPa}$.

Our analytical predictions are also included in Fig. 12 for comparison. Considering the average of both tests, the largest difference between experimental and analytical values is 9% for the elastic modulus and 8% for the compressive strength. Therefore, the measured properties are in good agreement with our analytical results and confirm that demi-regular lattices are slightly more compliant than a triangular lattice, but have a higher elastic buckling strength.

5. Conclusion

This study explored the potential of three demi-regular tessellations as stiff and strong lattice materials. Their in-plane mechanical properties were first derived analytically, then validated using Finite Element simulations, and corroborated by experiments performed on polymer lattices produced by additive manufacturing.

All three demi-regular tessellations had an in-plane isotropic and stretching-dominated behaviour. Consequently, their properties were compared to those of a triangular lattice, which exhibits the same characteristics. This comparison showed that demi-regular topologies are 5-20% more compliant, but up to 42% stronger than a triangular lattice when the failure mode is elastic buckling. With such combination of properties, demi-regular tessellations are attractive topologies for ultra-light and/or polymer lattices, which usually fail by elastic buckling of the constituent members.

There is growing evidence that prismatic lattices are not only stiff and strong, but also have a high fracture toughness [26–30]. Work is currently underway to evaluate if these three demi-regular tessellations are tougher than regular and semi-regular lattices.

Acknowledgements

AM wishes to thank the Finnish Cultural Foundation for their financial support (grant 00220662). LS is grateful for the funding received from the Academy of Finland (grant 322007).

A. Principle of minimum strain energy

A.1. Demi-regular lattice A

A.1.1. Loading in x_1

Using (3) to (6), we express T_2, T_3, T_4, and T_5 as functions of T_1, which yields:

$$T_2 = -\frac{T_1}{2}, \tag{A.1a}$$

$$T_3 = \frac{T_1}{2}, \tag{A.1b}$$

$$T_4 = -\frac{T_1}{2} + \frac{3\sqrt{3}}{4}\sigma_1 b\ell, \tag{A.1c}$$

$$T_5 = \frac{T_1}{2} + \frac{3\sqrt{3}}{4}\sigma_1 b\ell. \tag{A.1d}$$

Next, the strain energy for the unit cell shown in Fig. 3 is:

$$U = \frac{\ell}{2E_s bt}\left[6T_1^2 + 16T_2^2 + 8T_3^2 + 8T_4^2 + 4T_5^2\right], \tag{A.2}$$

and substituting (A.1) in (A.2) returns:

$$U = \frac{\ell}{2E_s bt}\left[15T_1^2 - 3\sqrt{3}T_1\sigma_1 b\ell + \frac{81}{4}(\sigma_1 b\ell)^2\right]. \tag{A.3}$$

The minimum strain energy is obtained by setting the derivative of U, with respect to T_1, equal to zero, which gives:

$$\frac{\partial U}{\partial T_1} = 0 \implies T_1 = \frac{\sqrt{3}}{10}\sigma_1 b\ell. \tag{A.4}$$

Finally, substituting (A.4) in (A.1) returns the internal forces in bars 2 to 5, and these are listed in (7).

A.1.2. Loading in x_2

First, we use (3), (4), (15) and (16) to express T_2, T_3, T_4, and T_5 as functions of T_1, which gives:

$$T_2 = -\frac{T_1}{2} + \frac{\sqrt{3}}{2}\sigma_2 b\ell, \tag{A.5a}$$

$$T_3 = \frac{T_1}{2} + \frac{\sqrt{3}}{2}\sigma_2 b\ell, \tag{A.5b}$$

$$T_4 = -\frac{T_1}{2} - \frac{\sqrt{3}}{4}\sigma_2 b\ell, \tag{A.5c}$$

$$T_5 = \frac{T_1}{2} - \frac{\sqrt{3}}{4}\sigma_2 b\ell. \tag{A.5d}$$

Second, we substitute these expressions in (A.2) to obtain the strain energy:

$$U = \frac{\ell}{2E_s bt}\left[15T_1^2 - 3\sqrt{3}T_1\sigma_2 b\ell + \frac{81}{4}(\sigma_2 b\ell)^2\right]. \tag{A.6}$$

Third, differentiating U with respect to T_1 to find the minimum strain energy yields:

$$\frac{\partial U}{\partial T_1} = 0 \implies T_1 = \frac{\sqrt{3}}{10}\sigma_2 b\ell. \tag{A.7}$$

Finally, substituting (A.7) in (A.5) returns the internal forces, which are given in (17).

A.2. Demi-regular lattice B

A.2.1. Loading in x_1

First, we express T_2, T_3, T_4, T_5 and T_6 as functions of T_1 using (22) to (25), which gives:

$$T_2 = T_1 + \frac{(1+\sqrt{3})}{2}\sigma_1 b\ell, \tag{A.8a}$$

$$T_3 = -T_1, \tag{A.8b}$$

$$T_4 = \frac{(3+\sqrt{3})}{6}\sigma_1 b\ell, \tag{A.8c}$$

$$T_5 = -T_1 + \frac{(1+\sqrt{3})}{4}\sigma_1 b\ell, \tag{A.8d}$$

$$T_6 = -\frac{(3+\sqrt{3})}{12}\sigma_1 b\ell. \tag{A.8e}$$

The strain energy for the unit cell illustrated in Fig. 4 is:

$$U = \frac{\ell}{2E_s bt}\left[8T_1^2 + 4T_2^2 + 8T_3^2 + 8T_4^2 + 4T_5^2 + 4T_6^2\right], \tag{A.9}$$

and substituting (A.8) into (A.9) yields:

$$U = \frac{\ell}{2E_s bt}\left[24T_1^2 + 2(1+\sqrt{3})T_1\sigma_1 b\ell + 4(2+\sqrt{3})(\sigma_1 b\ell)^2\right]. \tag{A.10}$$

Differentiating U with respect to T_1 and setting it equal to zero to find the minimum strain energy returns:

$$\frac{\partial U}{\partial T_1} = 0 \implies T_1 = -\frac{(1+\sqrt{3})}{24}\sigma_1 b\ell. \tag{A.11}$$

Finally, substituting this result in (A.8) gives the internal forces in bars 2 to 6, see (26).

A.2.2. Loading in x_2

Here, we use (21) to (23), (34) and (35) to express T_2, T_3, T_4, T_5, and T_6 as functions of T_1, which yields:

$$T_2 = T_1 - \frac{(1+\sqrt{3})}{2}\sigma_2 b\ell, \tag{A.12a}$$

$$T_3 = -T_1 + \frac{(1+\sqrt{3})}{2}\sigma_2 b\ell, \tag{A.12b}$$

$$T_4 = 0, \tag{A.12c}$$

$$T_5 = -T_1 + \frac{(1+\sqrt{3})}{4}\sigma_2 b\ell, \tag{A.12d}$$

$$T_6 = \frac{(3+\sqrt{3})}{4}\sigma_2 b\ell. \tag{A.12e}$$

Substituting these in (A.9) returns the strain energy:

$$U = \frac{\ell}{2E_s bt}\left[24T_1^2 - 14(1+\sqrt{3})T_1\sigma_2 b\ell + 8(2+\sqrt{3})(\sigma_2 b\ell)^2\right]. \tag{A.13}$$

Next, we differentiate this with respect to T_1 to find the minimum strain energy, and this gives:

$$\frac{\partial U}{\partial T_1} = 0 \implies T_1 = \frac{7(1+\sqrt{3})}{24}\sigma_2 b\ell. \tag{A.14}$$

Finally, substituting T_1 into (A.12) returns the internal forces given in (36).

A.3. Demi-regular lattice C

A.3.1. Loading in x_1

Using (40) to (47), we write $T_2, \ldots, T_9$ as functions of T_1, which gives:

$$T_2 = -\frac{1}{4}T_1 + \frac{(2+\sqrt{3})}{4}\sigma_1 b\ell, \tag{A.15a}$$

$$T_3 = \frac{\sqrt{3}}{4}T_1 + \frac{(3+2\sqrt{3})}{12}\sigma_1 b\ell, \tag{A.15b}$$

$$T_4 = -\frac{\sqrt{3}}{4}T_1 + \frac{(3+2\sqrt{3})}{4}\sigma_1 b\ell, \tag{A.15c}$$

$$T_5 = -\frac{1}{4}T_1, \tag{A.15d}$$

$$T_6 = -\frac{1}{4}T_1 + \frac{3(2+\sqrt{3})}{8}\sigma_1 b\ell, \tag{A.15e}$$

$$T_7 = \frac{\sqrt{3}}{4}T_1 - \frac{7(3+2\sqrt{3})}{24}\sigma_1 b\ell, \tag{A.15f}$$

$$T_8 = T_1 - \frac{(2+\sqrt{3})}{2}\sigma_1 b\ell, \tag{A.15g}$$

$$T_9 = -\frac{\sqrt{3}}{4}T_1 + \frac{(3+2\sqrt{3})}{8}\sigma_1 b\ell. \tag{A.15h}$$

Next, the strain energy for the unit cell in Fig. 5 is given by:

$$U = \frac{\ell}{2E_s bt}\left[2T_1^2 + 8(T_2^2 + T_3^2 + T_4^2 + T_5^2 + T_6^2) + 4(T_7^2 + T_8^2 + T_9^2)\right], \tag{A.16}$$

and substituting (A.15) in (A.16) yields:

$$U = \frac{\ell}{2E_s bt}\left[12T_1^2 - 11(2+\sqrt{3})T_1\sigma_1 b\ell + \frac{11(7+4\sqrt{3})}{2}(\sigma_1 b\ell)^2\right]. \tag{A.17}$$

Differentiating U with respect to T_1 and setting it equal to zero to find the minimum strain energy returns:

$$\frac{\partial U}{\partial T_1} = 0 \implies T_1 = \frac{11(2+\sqrt{3})}{24}\sigma_1 b\ell. \tag{A.18}$$

Finally, substituting this result in (A.15) returns the internal forces given in (48).

A.3.2. Loading in x_2

Here, we use (40) to (45), (56) and (57) to express $T_2, \ldots, T_9$ as functions of T_1, which yields:

$$T_2 = -\frac{1}{4}T_1, \tag{A.19a}$$

$$T_3 = \frac{\sqrt{3}}{4}T_1, \tag{A.19b}$$

$$T_4 = -\frac{\sqrt{3}}{4}T_1, \tag{A.19c}$$

$$T_5 = -\frac{1}{4}T_1 + \frac{(2+\sqrt{3})}{4}\sigma_2 b\ell, \tag{A.19d}$$

$$T_6 = -\frac{1}{4}T_1 - \frac{(2+\sqrt{3})}{8}\sigma_2 b\ell, \tag{A.19e}$$

$$T_7 = \frac{\sqrt{3}}{4}T_1 + \frac{3(3+2\sqrt{3})}{8}\sigma_2 b\ell, \tag{A.19f}$$

$$T_8 = T_1 + \frac{(2+\sqrt{3})}{2}\sigma_2 b\ell, \tag{A.19g}$$

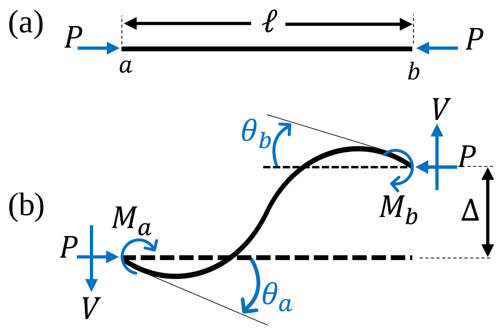

Figure B.1: (a) A bar of length ℓ subjected to a compressive load P. (b) The end rotations θ_a and θ_b generate bending moments M_a and M_b, respectively, and the transverse displacement Δ causes the shear force V.

$$T_9 = -\frac{\sqrt{3}}{4}T_1 + \frac{(3+2\sqrt{3})}{8}\sigma_2 b\ell. \tag{A.19h}$$

Next, we substitute (A.19) in (A.16), which gives:

$$U = \frac{\ell}{2E_s bt}\left[12T_1^2 + 5(2+\sqrt{3})\sigma_2 b\ell T_1 + \frac{7(7+4\sqrt{3})}{2}(\sigma_2 b\ell)^2\right]. \tag{A.20}$$

The minimum strain energy U allows us to find T_1, and this yields:

$$\frac{\partial U}{\partial T_1} = 0 \implies T_1 = -\frac{5(2+\sqrt{3})}{24}\sigma_2 b\ell. \tag{A.21}$$

Substituting this back in (A.19) returns the internal forces given in (58).

B. End constraint factor

Lattices with low relative densities usually fail by elastic buckling, and analytical predictions for this failure mode are sensitive to the end constraint factor n, see (1). The end constraint factor has been derived analytically for regular [6, 11] and semi-regular [21] lattices, and here, we extend this work to demi-regular lattices A, B, and C.

The method used to calculate the end constraint factor relies on the stiffness matrix of a single bar. Consider a bar of length ℓ loaded by an axial compressive force P, as shown in Fig. B.1a. Next, assume that small rotations θ_a and θ_b are imposed at ends a and b, respectively, and a small transverse displacement Δ is applied, see Fig. B.1b. The corresponding bending moments M_a and M_b, and shear force V are given by [31]:

$$\begin{Bmatrix} M_a \\ M_b \\ V \end{Bmatrix} = \frac{E_s I}{\ell} \begin{bmatrix} s & sc & \bar{s}/\ell \\ sc & s & \bar{s}/\ell \\ \bar{s}/\ell & \bar{s}/\ell & s^*/\ell^2 \end{bmatrix} \begin{Bmatrix} \theta_a \\ \theta_b \\ \Delta \end{Bmatrix}, \tag{B.1}$$

where E_s is the elastic modulus and I is the second moment of area of the bar. In addition, $\bar{s}$ and s^* are defined as:

$$\bar{s} = s(1+c) \quad \text{and} \quad s^* = 2\bar{s} - \frac{P\ell^2}{E_s I}, \tag{B.2}$$

in which parameters s and c vary depending on the axial load P. When the bar is loaded in compression ($P > 0$), s and c are given by:

$$s = \frac{\lambda(\sin\lambda - \lambda\cos\lambda)}{2 - 2\cos\lambda - \lambda\sin\lambda}, \tag{B.3}$$

and

$$c = \frac{\lambda - \sin\lambda}{\sin\lambda - \lambda\cos\lambda}, \tag{B.4}$$

where

$$\lambda = \sqrt{\frac{P}{E_s I}}\ell. \tag{B.5}$$

Otherwise, when the bar is in tension ($P < 0$), s and c have the form:

$$s = s_1 = \frac{\lambda_1(\lambda_1\cosh\lambda_1 - \sinh\lambda_1)}{2 - 2\cosh\lambda_1 + \lambda_1\sinh\lambda_1}, \tag{B.6}$$

$$c = c_1 = \frac{\sinh\lambda_1 - \lambda_1}{\lambda_1\cosh\lambda_1 - \sinh\lambda_1}, \tag{B.7}$$

$$\lambda_1 = \sqrt{\frac{\text{-}P}{E_s I}}\ell, \tag{B.8}$$

where the subscript 1 is used simply to differentiate these expressions from those in (B.3) to (B.5). Finally, when the bar carries no axial load ($P = 0$), the parameters s and c are:

$$s = 4 \quad \text{and} \quad c = 0.5. \tag{B.9}$$

The approach to find the end constraint factor n is as follows. First, the periodic buckling shape with the longest wavelength is identified for each topology and for each loading direction. Then, equilibrium conditions and (B.1) are combined to form a constitutive equation from which λ can be solved. Once λ is known, it is straightforward to compute the end constraint factor n since $\lambda = \pi n$.

B.1. Demi-regular lattice A

First, consider demi-regular lattice A compressed in the x_1 direction. For this loading scenario, the periodic buckling shape illustrated in Fig. B.2a is the one associated with the lowest load. This pattern has two rotations, denoted as θ_1 and θ_2, whereas there are no rotations at vertices b and d. By equilibrium, the bending moments at vertices a and f are zero, and this gives:

$$M_{ab} + M_{ac} + M_{ad} + M_{ae} + M_{ak} = 0, \tag{B.10a}$$

$$2M_{fb} + 2M_{fc} + M_{fg} = 0, \tag{B.10b}$$

respectively. Here, the notation M_{ij} denotes the bending moment in bar ij at end i. Each term in (B.10) is expressed as a function of θ_1 and θ_2 using (B.1), and this returns:

$$M_{ab} = \frac{E_s I}{\ell}\left(s_{1ab}\theta_2\right), \tag{B.11a}$$

$$M_{ac} = \frac{E_s I}{\ell}\left(s_{ac}\theta_2 - s_{ac}c_{ac}\theta_2\right), \tag{B.11b}$$

$$M_{ad} = \frac{E_s I}{\ell}\left(s_{ad}\theta_2\right), \tag{B.11c}$$

$$M_{ae} = \frac{E_s I}{\ell}\left(s_{ae}\theta_2 - s_{ae}c_{ae}\theta_2\right), \tag{B.11d}$$

$$M_{ak} = \frac{E_s I}{\ell}\left(s_{ak}\theta_2 - s_{ak}c_{ak}\theta_1\right), \tag{B.11e}$$

$$M_{fb} = \frac{E_s I}{\ell}\left(s_{1fb}\theta_1\right), \tag{B.11f}$$

$$M_{fc} = \frac{E_s I}{\ell}\left(s_{fc}\theta_1 - s_{fc}c_{fc}\theta_2\right), \tag{B.11g}$$

$$M_{fg} = \frac{E_s I}{\ell}\left(s_{fg}\theta_1 - s_{fg}c_{fg}\theta_1\right), \tag{B.11h}$$

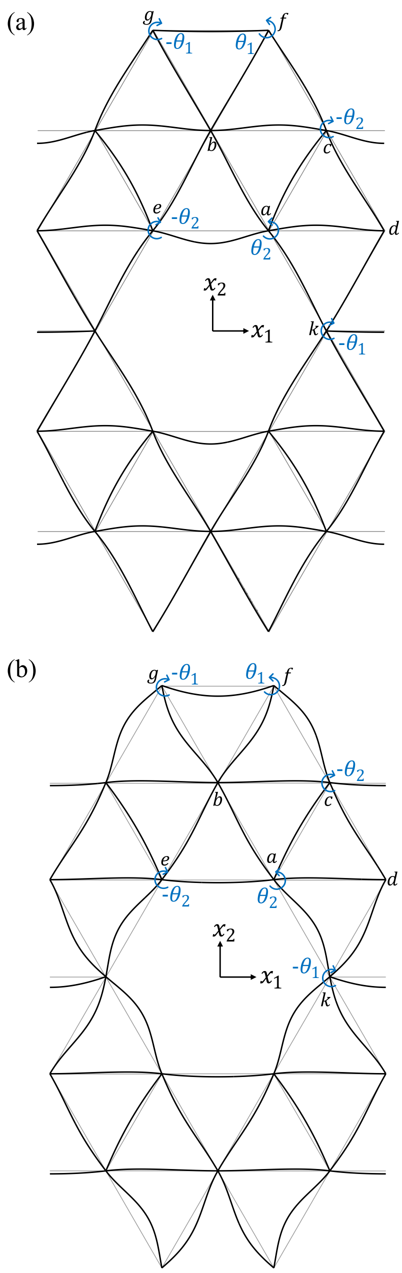

Figure B.2: Periodic buckling modes of demi-regular lattice A compressed in (a) x_1 and (b) x_2.

where s_{ij} and c_{ij} are functions of λ_{ij} as defined in relations (B.3) to (B.9). Each λ_{ij} is proportional to the axial force in bar ij (see (B.5)); therefore, with the internal loads in (7), we find that:

$$\lambda_{ad} = 0.9354\lambda_{ae}, \tag{B.12a}$$

$$\lambda_{ac} = \lambda_{fg} = 0.3536\lambda_{ae}, \tag{B.12b}$$

$$\lambda_{1ab} = \lambda_{1fb} = 0.25\lambda_{ae}, \tag{B.12c}$$

$$\lambda_{ak} = \lambda_{fc} = 0.25\lambda_{ae}. \tag{B.12d}$$

Above, each λ_{ij} is expressed as a function of λ_{ae} since bar ae is the most loaded strut and the one expected to buckle. Substituting (B.11) in (B.10) returns a linear system of equations: $\boldsymbol{A}[\theta_1, \theta_2]^T = \boldsymbol{0}$, where the determinant of $\boldsymbol{A}$ should be zero for a non-trivial solution to exists. With the expressions in (B.12), setting $\det(\boldsymbol{A}) = 0$ returns a lengthy expression where λ_{ae} is the only unknown. Solving numerically yields $\lambda_{ae} = 5.131$ and therefore, the end constraint factor for compression in x_1 is:

$$n_1 = \frac{\lambda_{ae}}{\pi} = 1.633. \tag{B.13}$$

Next, consider demi-regular lattice A compressed in the x_2 direction. In this case, the lattice collapses according to the periodic buckling shape shown in Fig. B.2b. Equation (B.10) remain valid, but the bending moments are now given by:

$$M_{ab} = \frac{E_s I}{\ell}\left(s_{ab}\theta_2\right), \tag{B.14a}$$

$$M_{ac} = \frac{E_s I}{\ell}\left(s_{ac}\theta_2 - s_{ac}c_{ac}\theta_2\right), \tag{B.14b}$$

$$M_{ad} = \frac{E_s I}{\ell}\left(s_{1ad}\theta_2\right), \tag{B.14c}$$

$$M_{ae} = \frac{E_s I}{\ell}\left(s_{1ae}\theta_2 - s_{1ae}c_{1ae}\theta_2\right), \tag{B.14d}$$

$$M_{ak} = \frac{E_s I}{\ell}\left(s_{ak}\theta_2 - s_{ak}c_{ak}\theta_1\right), \tag{B.14e}$$

$$M_{fb} = \frac{E_s I}{\ell}\left(s_{fb}\theta_1\right), \tag{B.14f}$$

$$M_{fc} = \frac{E_s I}{\ell}\left(s_{fc}\theta_1 - s_{fc}c_{fc}\theta_2\right), \tag{B.14g}$$

$$M_{fg} = \frac{E_s I}{\ell}\left(s_{fg}\theta_1 - s_{fg}c_{fg}\theta_1\right), \tag{B.14h}$$

where the parameters s_{ij} and c_{ij} are again functions of λ_{ij}. Next, we use the internal loads in (17) to express each λ_{ij} as a function of λ_{fc} since this is the bar sustaining the highest force and expected to buckle. This gives:

$$\lambda_{ak} = \lambda_{fc}, \tag{B.15a}$$

$$\lambda_{ac} = \lambda_{fg} = 0.4264\lambda_{fc}, \tag{B.15b}$$

$$\lambda_{ab} = \lambda_{fb} = 0.9045\lambda_{fc}, \tag{B.15c}$$

$$\lambda_{1ad} = 0.7385\lambda_{fc}, \tag{B.15d}$$

$$\lambda_{1ae} = 0.6030\lambda_{fc}. \tag{B.15e}$$

Similarly to the analysis in x_1, substituting (B.14) in (B.10) returns a linear system of equations: $\boldsymbol{A}[\theta_1, \theta_2]^T = \boldsymbol{0}$, where the determinant of $\boldsymbol{A}$ should be zero for a non-trivial solution to exists. Setting $\det(\boldsymbol{A}) = 0$, and using the relations in (B.15), returns an expression where λ_{fc} is the only unknown. Solving numerically gives $\lambda_{fc} = 4.5697$ and therefore, the end constraint factor in x_2 is:

$$n_2 = \frac{\lambda_{fc}}{\pi} = 1.4546. \tag{B.16}$$

B.2. Demi-regular lattice B

When compressed in x_1, demi-regular lattice B buckles according to the periodic pattern shown in Fig. B.3a. This mode is characterised by three rotations denoted θ_1, θ_2 and θ_3. Equilibrium of moments at vertices a, b and k gives:

$$M_{ab} + M_{ac} + M_{ad} + M_{ae} + M_{af} = 0, \tag{B.17a}$$

$$M_{ba} + M_{bc} + M_{bk} + M_{bg} + M_{bh} = 0, \tag{B.17b}$$

$$M_{kb} + M_{kg} + M_{kh} = 0, \tag{B.17c}$$

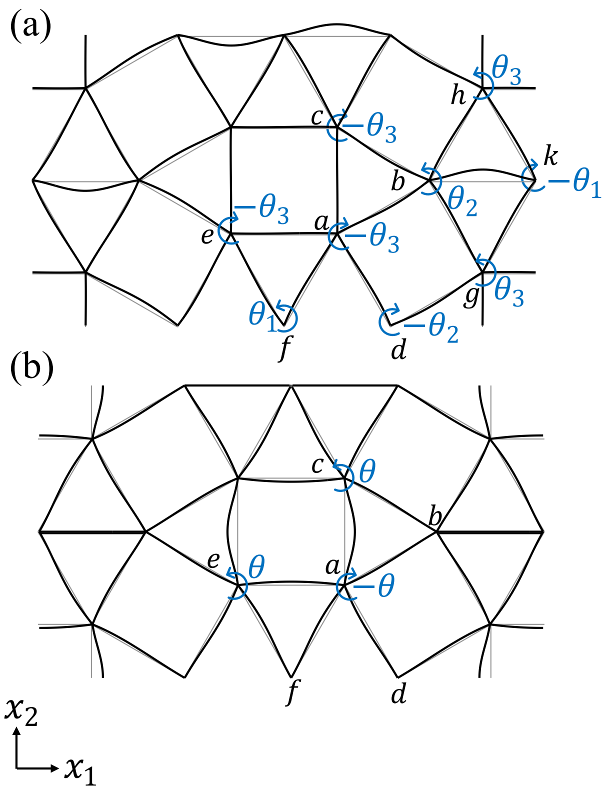

Figure B.3: Periodic buckling modes of demi-regular lattice B compressed in (a) x_1 and (b) x_2.

respectively, where each bending moment is expressed as a function of θ_1, θ_2 and θ_3 using (B.1), which yields:

$$M_{ab} = \frac{E_s I}{\ell} \left(-s_{ab}\theta_3 + s_{ab}c_{ab}\theta_2\right), \tag{B.18a}$$

$$M_{ac} = \frac{E_s I}{\ell} \left(-s_{1ac}\theta_3 - s_{1ac}c_{1ac}\theta_3\right), \tag{B.18b}$$

$$M_{ad} = \frac{E_s I}{\ell} \left(-s_{ad}\theta_3 - s_{ad}c_{ad}\theta_2\right), \tag{B.18c}$$

$$M_{ae} = \frac{E_s I}{\ell} \left(-s_{ae}\theta_3 - s_{ae}c_{ae}\theta_3\right), \tag{B.18d}$$

$$M_{af} = \frac{E_s I}{\ell} \left(-s_{1af}\theta_3 + s_{1af}c_{1af}\theta_1\right), \tag{B.18e}$$

$$M_{ba} = \frac{E_s I}{\ell} \left(s_{ba}\theta_2 - s_{ba}c_{ba}\theta_3\right), \tag{B.18f}$$

$$M_{bc} = \frac{E_s I}{\ell} \left(s_{bc}\theta_2 - s_{bc}c_{bc}\theta_3\right), \tag{B.18g}$$

$$M_{bk} = \frac{E_s I}{\ell} \left(s_{bk}\theta_2 - s_{bk}c_{bk}\theta_1\right), \tag{B.18h}$$

$$M_{bg} = \frac{E_s I}{\ell} \left(s_{bg}\theta_2 + s_{bg}c_{bg}\theta_3 \right), \tag{B.18i}$$

$$M_{bh} = \frac{E_s I}{\ell} \left(s_{bh}\theta_2 + s_{bh}c_{bh}\theta_3 \right), \tag{B.18j}$$

$$M_{kb} = \frac{E_s I}{\ell} \left(-s_{kb}\theta_1 + s_{kb}c_{kb}\theta_2 \right), \tag{B.18k}$$

$$M_{kg} = \frac{E_s I}{\ell} \left(-s_{1kg}\theta_1 + s_{1kg}c_{1kg}\theta_3 \right), \tag{B.18l}$$

$$M_{kh} = \frac{E_s I}{\ell} (-s_{1kh}\theta_1 + s_{1kh}c_{1kh}\theta_3). \tag{B.18m}$$

Above, the parameters s_{ij} and c_{ij} are functions of λ_{ij} as defined in (B.3) to (B.9). Each λ_{ij} is proportional to the axial force in bar ij and, with the internal loads in (26), we find that:

$$\lambda_{bg} = \lambda_{bh} = \lambda_{ad} = 0.3015\lambda_{kb}, \tag{B.19a}$$

$$\lambda_{ab} = \lambda_{bc} = 0.7936\lambda_{kb}, \tag{B.19b}$$

$$\lambda_{ae} = 0.7977\lambda_{kb}, \tag{B.19c}$$

$$\lambda_{1ac} = 0.5612\lambda_{kb}, \tag{B.19d}$$

$$\lambda_{1af} = \lambda_{1kg} = \lambda_{1kh} = 0.3015\lambda_{kb}, \tag{B.19e}$$

where all λ_{ij} are expressed as functions of λ_{kb} since this is the most loaded strut and the one expected to buckle. To find λ_{kb}, we first substitute (B.18) in (B.17) to form a system of equations: $\boldsymbol{A}[\theta_1, \theta_2, \theta_3]^T = \mathbf{0}$. Next, we set $\det(\boldsymbol{A}) = 0$ and use (B.19) to obtain an expression as a function of λ_{kb} only. Solving this expression numerically returns $\lambda_{kb} = 5.1839$ and consequently, the end constraint factor in x_1 is:

$$n_1 = \frac{\lambda_{kb}}{\pi} = 1.650. \tag{B.20}$$

Next, consider demi-regular lattice B compressed in the x_2 direction. In this case, the lattice is expected to deform according to the periodic buckling shape shown in Fig. B.3b. Equilibrium of vertex a gives:

$$M_{ab} + M_{ac} + M_{ad} + M_{ae} + M_{af} = 0, \tag{B.21}$$

where each bending moment is:

$$M_{ab} = \frac{E_s I}{\ell} \left(-s_{ab}\theta \right), \tag{B.22a}$$

$$M_{ac} = \frac{E_s I}{\ell} \left(-s_{ac}\theta + s_{ac}c_{ac}\theta \right), \tag{B.22b}$$

$$M_{ad} = \frac{E_s I}{\ell} \left(-s_{ad}\theta \right), \tag{B.22c}$$

$$M_{ae} = \frac{E_s I}{\ell} \left(-s_{1ae}\theta + s_{1ae}c_{1ae}\theta \right), \tag{B.22d}$$

$$M_{af} = \frac{E_s I}{\ell} \left(-s_{af}\theta \right). \tag{B.22e}$$

Note that $s_{ab} = 4$ because bar ab carries no load, see (36) and (B.9). Otherwise, each λ_{ij} is expressed as a function λ_{ac} (since this is the most loaded bar and the one expected to buckle) using the internal loads in (36), which gives:

$$\lambda_{ad} = 0.6936\lambda_{ac}, \tag{B.23a}$$

$$\lambda_{1ae} = 0.3102\lambda_{ac}, \tag{B.23b}$$

$$\lambda_{af} = 0.8207\lambda_{ac}. \tag{B.23c}$$

Substituting (B.22) in (B.21), and then making use of (B.23), returns a lengthy expression where λ_{ac} is the only unknown. Solving numerically returns $\lambda_{ac} = 5.2149$ and therefore, the end constraint factor in x_2 is:

$$n_2 = \frac{\lambda_{ac}}{\pi} = 1.659. \tag{B.24}$$

B.3. Demi-regular lattice C

When compressed in the x_1 direction, demi-regular lattice C buckles in the periodic pattern shown in Fig. B.4a. This deformation mode is characterised by two rotations (θ_1 and θ_2), whereas there is no rotation at vertices d and h. Equilibrium of vertices a and c gives:

$$2M_{ad} + 2M_{ae} + M_{af} = 0, \tag{B.25a}$$

$$M_{cg} + M_{ch} + M_{ck} + M_{cl} + M_{cm} = 0, \tag{B.25b}$$

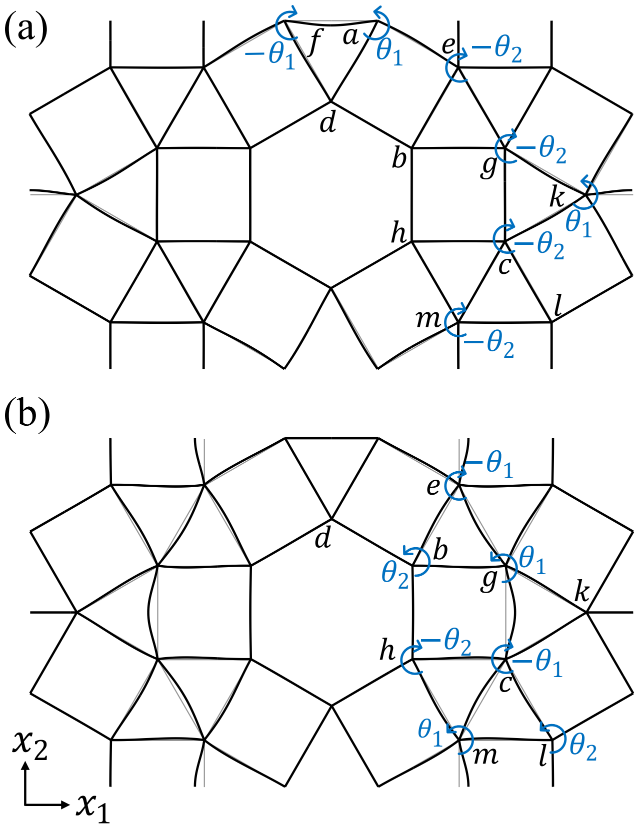

Figure B.4: Periodic buckling modes of demi-regular lattice C compressed in (a) x_1 and (b) x_2.

respectively, where the bending moments are:

$$M_{ad} = \frac{E_s I}{\ell}\left(s_{ad}\theta_1\right), \tag{B.26a}$$

$$M_{ae} = \frac{E_s I}{\ell}\left(s_{ae}\theta_1 - s_{ae}c_{ae}\theta_2\right), \tag{B.26b}$$

$$M_{af} = \frac{E_s I}{\ell}\left(s_{af}\theta_1 - s_{af}c_{af}\theta_1\right), \tag{B.26c}$$

$$M_{cg} = \frac{E_s I}{\ell}\left(-s_{1cg}\theta_2 - s_{1cg}c_{1cg}\theta_2\right), \tag{B.26d}$$

$$M_{ch} = \frac{E_s I}{\ell}\left(-s_{ch}\theta_2\right), \tag{B.26e}$$

$$M_{ck} = \frac{E_s I}{\ell}\left(-s_{ck}\theta_2 + s_{ck}c_{ck}\theta_1\right), \tag{B.26f}$$

$$M_{cl} = \frac{E_s I}{\ell}\left(-s_{1cl}\theta_2\right), \tag{B.26g}$$

$$M_{cm} = \frac{E_s I}{\ell}\left(-s_{1cm}\theta_2 - s_{1cm}c_{1cm}\theta_2\right). \tag{B.26h}$$

Again, substituting (B.26) in (B.25), then setting the determinant of the coefficient matrix to zero, and making use of the following relations:

$$\lambda_{ad} = 0.5436\lambda_{af}, \tag{B.27a}$$

$$\lambda_{ae} = \lambda_{ck} = 0.8648\lambda_{af}, \tag{B.27b}$$

$$\lambda_{1cg} = 0.8180\lambda_{af}, \tag{B.27c}$$

$$\lambda_{ch} = 0.7538\lambda_{af}, \tag{B.27d}$$

$$\lambda_{1cl} = 0.5\lambda_{af}, \tag{B.27e}$$

$$\lambda_{1cm} = 0.3015\lambda_{af}, \tag{B.27f}$$

returns an expression where λ_{af} is the only unknown. Solving numerically, we find $\lambda_{af} = 4.922$ and hence, the end constraint factor in x_1 is:

$$n_1 = \frac{\lambda_{af}}{\pi} = 1.567. \tag{B.28}$$

Finally, consider demi-regular lattice C compressed in the x_2 direction. In this case, the lattice collapses according to the periodic buckling shape shown in Fig. B.4b. Equilibrium of vertices b and c implies:

$$M_{bd} + M_{be} + M_{bg} + M_{bh} = 0, \tag{B.29a}$$

$$M_{cg} + M_{ch} + M_{ck} + M_{cl} + M_{cm} = 0, \tag{B.29b}$$

respectively, where the bending moments are:

$$M_{bd} = \frac{E_s I}{\ell}\left(s_{bd}\theta_2\right), \tag{B.30a}$$

$$M_{be} = \frac{E_s I}{\ell}\left(s_{be}\theta_2 - s_{be}c_{be}\theta_1\right), \tag{B.30b}$$

$$M_{bg} = \frac{E_s I}{\ell}\left(s_{1bg}\theta_2 + s_{1bg}c_{1bg}\theta_1\right), \tag{B.30c}$$

$$M_{bh} = \frac{E_s I}{\ell}\left(s_{bh}\theta_2 - s_{bh}c_{bh}\theta_2\right), \tag{B.30d}$$

$$M_{cg} = \frac{E_s I}{\ell}\left(-s_{cg}\theta_1 + s_{cg}c_{cg}\theta_1\right), \tag{B.30e}$$

$$M_{ch} = \frac{E_s I}{\ell}\left(-s_{1ch}\theta_1 - s_{1ch}c_{1ch}\theta_2\right), \tag{B.30f}$$

$$M_{ck} = \frac{E_s I}{\ell}\left(-s_{1ck}\theta_1\right), \tag{B.30g}$$

$$M_{cl} = \frac{E_s I}{\ell}\left(-s_{cl}\theta_1 + s_{cl}c_{cl}\theta_2\right), \tag{B.30h}$$

$$M_{cm} = \frac{E_s I}{\ell}\left(-s_{cm}\theta_1 + s_{cm}c_{cm}\theta_1\right), \tag{B.30i}$$

where s_{ij} and c_{ij} are defined in (B.3) to (B.9). Substituting (B.30) in (B.29) gives a system of equations: $\boldsymbol{A}[\theta_1, \theta_2]^T = \mathbf{0}$. Next, setting $\det(\boldsymbol{A}) = 0$ and making use of the following relations:

$$\lambda_{bd} = \lambda_{1ck} = 0.4016\lambda_{cg}, \tag{B.31a}$$

$$\lambda_{be} = \lambda_{cl} = 0.7349\lambda_{cg}, \tag{B.31b}$$

$$\lambda_{1bg} = \lambda_{1ch} = 0.3611\lambda_{cg}, \tag{B.31c}$$

$$\lambda_{bh} = 0.7405\lambda_{cg}, \tag{B.31d}$$

$$\lambda_{cm} = 0.7221\lambda_{cg}, \tag{B.31e}$$

returns an expression where λ_{cg} is the only unknown. Solving numerically gives $\lambda_{cg} = 5.237$ and we find that the end constraint factor for compression in x_2 is:

$$n_2 = \frac{\lambda_{cg}}{\pi} = 1.667. \tag{B.32}$$

References

[1] Evans AG, Hutchinson JW, Fleck NA, Ashby MF, Wadley HNG. The topological design of multifunctional cellular metals. Prog Mater Sci 2001;46:309–27.

[2] Seepersad CC, Dempsey BM, Allen JK, Mistree F, McDowel DL. Design of multifunctional honeycomb materials. AIAA J 2004;42:1025–33.

[3] Gibson LJ, Ashby MF. Cellular solids: structure and properties. 2nd ed.; Cambridge University Press; 1997.

[4] Torquato S, Gibiansky LV, Silva MJ, Gibson LJ. Effective mechanical and transport properties of cellular solids. Int J Mech Sci 1998;40(1):71–82.

[5] Wang AJ, McDowell DL. In-plane stiffness and yield strength of periodic metal honeycombs. J Eng Mater Technol 2004;126(2):137–56.

[6] Fan H, Jin F, Fang D. Uniaxial local buckling strength of periodic lattice composites. Mater Des 2009;30(10):4136–45.

[7] Tankasala HC, Deshpande VS, Fleck NA. Tensile response of elastoplastic lattices at finite strain. J Mech Phys Solids 2017;109:307–30.

[8] Papka SD, Kyriakides S. In-plane compressive response and crushing of honeycomb. J Mech Phys Solids 1994;42(10):1499–532.

[9] Côté F, Deshpande VS, Fleck NA, Evans AG. The compressive and shear responses of corrugated and diamond lattice materials. Int J Solids Struct 2006;43(20):6220–42.

[10] Gu H, Pavier M, Shterenlikht A. Experimental study of modulus, strength and toughness of 2D triangular lattices. Int J Solids Struct 2018;152–153:207–16.
[11] Markou A, St-Pierre L. A novel parameter to tailor the properties of prismatic lattice materials. Int J Mech Sci 2022;:107079.
[12] Deshpande VS, Ashby MF, Fleck NA. Foam topology: bending versus stretching dominated architectures. Acta Mater 2001;49(6):1035–40.
[13] Williams R. The geometrical foundation of natural structure: a source book of design. Dover, New York; 1979.
[14] Grünbaum B, Shephard GC. Tilings and patterns. Dover, New York; 1987.
[15] Hyun S, Torquato S. Optimal and manufacturable two-dimensional, Kagomé-like cellular solids. J Mater Res 2002;17(1):137–44.
[16] Hutchinson RG, Wicks N, Evans AG, Fleck NA, Hutchinson JW. Kagome plate structures for actuation. Int J Solids Struct 2003;40(25):6969–80.
[17] Symons DD, Hutchinson RG, Fleck NA. Actuation of the kagome double-layer grid. Part 1: prediction of performance of the perfect structure. J Mech Phys Solids 2005;53(8):1855–74.
[18] Elsayed MSA, Pasini D. Analysis of the elastostatic specific stiffness of 2D stretching-dominated lattice materials. Mech Mater 2010;42(7):709–25.
[19] Pronk TN, Ayas C, Tekõglu C. A quest for 2D lattice materials for actuation. J Mech Phys Solids 2017;105:199–216.
[20] Their T, St-Pierre L. Stiffness and strength of a semi-regular lattice. Raken Mek 2017;50(3):137–40.
[21] Omidi M, St-Pierre L. Mechanical properties of semi-regular lattices. Mater Des 2022;:110324.
[22] Romijn NE, Fleck NA. The fracture toughness of planar lattices: Imperfection sensitivity. J Mech Phys Solids 2007;55(12):2538–64.
[23] Symons DD, Fleck NA. The imperfection sensitivity of isotropic two-dimensional elastic lattices. J Appl Mech 2008;75(5):051011.
[24] Christensen RM. Sufficient symmetry conditions for isotropy of the elastic moduli tensor. J Appl Mech 1987;54:772–777.
[25] Timoshenko S, Gere JM. Theory of elasticity stability. New York: McGraw-Hill; 1961.
[26] Liu Y, St-Pierre L, Fleck NA, Deshpande VS, Srivastava A. High fracture toughness micro-architectured materials. J Mech Phys Solids 2020;143:104060.
[27] Hsieh MT, Deshpande VS, Valdevit L. A versatile numerical approach for calculating the fracture toughness and R-curves of cellular materials. J Mech Phys Solids 2020;138:103925.
[28] Tankasala HC, Fleck NA. The crack growth resistance of an elastoplastic lattice. Int J Solids Struct 2020;188-189:233–43.
[29] Shu X, Mao Y, Lei M, Da D, Hou S, Zhang P. Toughness enhancement of honeycomb lattice structures through heterogeneous design. Mater Des 2022;217:110604.
[30] Omidi M, St-Pierre L. Fracture toughness of semi-regular lattices. Int J Solids Struct 2023;270:112233.
[31] Bažant Z, Cedolin L. Stability of structures: elastic, inelastic, fracture and damage theories. New York: Oxford University Press; 1991.